Øystein Thordén Haug

The Effect of Fragmentation on Gravitational Rock Movements

Dissertation zur Erlangung des Doktorgrades im
Fachbereich Geowissenschaften
an der
Freien Universität Berlin

Berlin, 2015

The Effect of Fragmentation on Gravitational Rock Movements

A Dissertation submitted in partial fulfilment of the requirements for the degree:

Doctor of Natural Sciences in the field of Earth Sciences

to the department of Geowissenschaften of the Freie Universität Berlin.

Author

Øystein Thordén Haug

Place and date of submission:

Berlin, April 2015

Erstgutachter: Prof. Dr. Onno Oncken
Freien Universität Berlin, GeoForschungsZentrum Potsdam

Zweitgutachter: Prof. Dr. Niels Hovius
Universität Potsdam, GeoForschungsZentrum Potsdam

Drittgutachter: Prof. Dr. Rupert Klein
Universität Potsdam

Tag der Disputation: 10.07.2015

Abstract

Rock slides and avalanches, and gravitational mass movements in general, are not well understood geological phenomena, the simulation of which is difficult because of the complexity and multitude of acting processes. After mechanical failure of a rock slope, the rocks are transported by gravity and emplaced somewhere downslope. How that transport occurs, and how far the material is transported is determined by numerous processes, working simultaneously across a large range of scales, making prediction of the system behavior difficult. One of these processes is fragmentation, which by breaking the material apart can change the dynamic properties of the rock mass by transforming the intact rock mass into a flowing granular material, as well as potentially changing the effective basal friction. Despite this, fragmentation is rarely considered in studies of gravitational rock movement.

Previous studies on fragmentation in gravitational rock movements have mainly considered the final deposits. Thus, little is known of the conditions under which the fragmentation occurred, and how it affected the movement. Observations of these systems as they occur in nature, at sufficient temporal and spatial resolution are hard to come by, and modeling serves as an important tool to constrain the physics of their transport. Existing models rarely take the process of fragmentation into account, assuming instead that the movement can be approximated with constant material properties throughout the transport event.

Here, a new experimental approach is presented where the fragmentation of a rock analogue material during transport down a chute is considered at lab-scale.

The analogue material used in the models is produced by cementing sand with either gypsum or potato starch. The cement provides the material with a cohesion, which if loaded above a failure criterion is lost. Material testing using a ring shear tester and a triaxial tester reveal that the cohesion of the material is determined by the amount and type of cement added, such that the cohesion can be controlled from 3.5 ± 2.2 to 360 ± 72 kPa.

Rock slides and avalanches are modeled by releasing a cuboid-shaped block of the analogue material down a 1 m slope, at an angle of 45°. After accelerating down the slope, the blocks impact on a horizontal plate, on which they fragment, slide and come to rest. The models are scaled to nature by considering a set of characterizing dimensionless parameters derived from dimensional analysis. Of these parameters, the aspect ratio of the sliding material, the cohesion versus potential energy ratio and the basal coefficient of friction are studied in a parameter study.

The parameter study reveals that the degree of fragmentation increases the thicker the

sample is compared to its length, or if its strength increases with respect to its initial potential energy. The relative contribution of these two parameters on the degree of fragmentation is considered through an analytical model of an elastic bending plate. Based on this model, a new parameter is suggested which can be used to predict the degree of fragmentation solely from initial conditions, taking into account the geometry, rock strength and potential energy.

The fragmentation is observed to consume energy, causing a reduced transport of the center of mass. An analysis based on the conservation of energy suggests that the energy consumed by fragmentation can be described by a logarithmic scaling law. Despite the loss of energy, fragmentation is observed to cause spreading of the material, leading to an increased travel distance of the front position of the deposits.

However, the front position is seen to depend on the degree of fragmentation in a complex manner, increasing for intermediate degrees of fragmentation but decreasing for higher ones. Careful observations of the analogue models suggest this behavior to be caused by a competition between spreading and increased internal friction. Because of this competition, an intermediately fragmented rock, i.e. a fragmenting strong rock, is expected to have a higher mobility than a highly fragmented one, i.e. a collapsing weak rock.

A comparison between the mobility as a function of the degree of fragmentation from the analogue model and a data set of natural rock avalanches reveal a remarkably good fit between model and nature and thereby the models applicability. This shows that fragmentation is a governing process in the transport of rock avalanches, and for gravitational rock movements in general.

Zusammenfassung

Gesteinsrutschungen und -lawinen, bzw. gravitative Massenbewegungen im allgemeinen, gehören zu den wenig verstandenen geologischen Phänomenen, deren Simulation aufgrund der Komplexität und Vielzahl der beteiligten Prozesse schwierig ist. Nach dem mechanischen Versagen eines Hanges aus Gestein werden Gesteine gravitativ bewegt und hangabwärts abgelagert. Wie dieser Transport stattfindet und wie weit das Material transportiert wird, wird durch eine Reihe von Prozessen gesteuert, die zeitgleich und auf verschiedenen Skalen arbeiten, und so die Vorhersage des Systemverhaltens schwierig gestalten.

Einer dieser ablaufenden Prozesse ist Fragmentierung, der zu Separierung und dadurch zu einer Änderung der dynamischen Eigenschaften der Gesteinsmasse führt, indem er intaktes Gestein in ein fliessendes granulares Material verwandelt und möglicherweise auch die effektive Reibung an der Basis vermindert. Trotz dieses Einflusses findet Fragmentierung wenig Beachtung in Studien zu gravitativen Massenbewegungen.

Vorhergehende Studien zu Fragmentierung in gravitativen Massenbewegungen untersuchten meist die finale Ablagerungen. Demzufolge ist wenig verstanden unter welchen Bedingungen Fragmentierung ensteht und wie es die Bewegung beeinflusst.

Beobachtung aktiver Massenbewegungen in der Natur in ausreichender zeitlicher und räumlicher Auflösung ist kaum möglich. Modellierung hilft hier als ein wichtiges Werkzeug, um die Physik des Transportes zu untersuchen.

Existierende Modelle berücksichtigen selten den Fragmentierungsprozess und nehmen an, dass die Bewegung durch konstante Materialeigenschaften während des Transportes angenähert werden kann.

In dieser Arbeit wird ein neuer experimenteller Ansatz präsentiert, in dem Fragmentierung eines analogen Gesteinsmaterials während des Transport entlang einer Schütte als labormaßstäbliches Analogmodell für den oben beschrieben Prozess gilt.

Das in den Modellen benutzte Analogmaterial besteht aus zementierten Sand. Als Zement dienen Gips oder Kartoffelstärke. Der Zement verleiht dem Material die nötige Kohäsion, die bei Belastung über ein Bruchkriterium hinaus verloren geht. Materialprüfungen mittels Ringschergerät und Triax-Versuch zeigen, dass die Kohäsion bestimmt wird durch die Menge und Art des Zementes, sodass die Kohäsion über zwei Größenordnungen variiert werden kann, von 3,5 bis 360 kPa.

Gesteinsrutschungen und -lawinen werden hier durch einen quaderförmigen Block des Analogmaterials modelliert, der eine 1 Meter lange und 45° geneigte Ebene hinabgleitet. Nach

der Beschleunigung auf der schiefen Ebene prallt der Block auf eine horizontale Platte, auf der er fragmentiert, weiter rutscht und schließlich zum Stillstand kommt.

Die Modelle sind bezüglich der Natur skaliert gemäß eines Satzes charakteristischer dimensionsloser Parameter, die aus einer Dimensionsanalyse folgen. Von diesen Parametern werden in dieser Studie die Rolle des Verhältnises von Kohäsion zu potentieller Energy sowie des basalen Reibungskoeffizientes systematisch untersucht.

Die Parameterstudie zeigt, dass der Fragmentierungsgrad mit der auf die Länge normierten Dicke der Probe korreliert bzw. zunimmt wenn die Festigkeit im Verhältnis zur potentiellen Energie ansteigt. Der relative Beitrag dieser beiden Parameter zur Fragmentierung wird mittels eines analytischen Modells einer elastischen, sich biegenden Platte betrachtet. Basierend auf diesem Modell wird ein neuer Parameter vorgeschlagen, der es erlaubt den Fragmentierungsgrad alleine aus Ausgangsbedingungen (Geometrie, Festigkeit, potentielle Energie) vorherzusagen.

Fragmentierung zeigt sich als Energieverbraucher, was eine reduzierte Transportweite des Schwerpunktes zur Folge hat. Eine Analyse basierend auf Energieerhaltung zeigt, dass die Energie, die bei Fragmentierung verloren geht durch eine logarhytmisches Skalierungsgesetz beschrieben werden kann. Trotz Energieverlust erzeugt Fragmentierung eine Streuung des Materials, die eine erhöhte Auslaufweite der Front der Ablagerung zur Folge hat.

Jedoch zeigt sich, dass die Frontposition in komplexer Weise vom Fragmentierungsgrad abhängt: Sie steigt bis zu mittleren Fragmentierungsgrade an um darüber hinaus wieder abzufallen. Genaue Beobachtung des Analogmodels legt nahe, dass dieses Verhalten durch einen Wettbewerb zwischen Streuung und erhöhter interner Reibung kontroliert wird. Wegen dieses Wettbewerbs wird ein mittelstark fragmentierendes, also festes Gestein eine höhere Mobilität haben als ein hoch fragmentiertes, also schwaches Gestein.

Ein Vergleich zwischen der Mobilität als Funktion des Fragmentierungsgrade im Analogmodell mit der Natur deutet gute Vergleichbarkeit und Anwendbarkeit an. Dies zeigt, dass Fragmentierung ein bestimmender Prozess im Transport von Gesteinsrutschungen, -lawinen und gravitativen Massenbewegungen im allgemeinen ist.

Contents

Chapter 1

Introduction

Rockslides and rockfalls are hazards potentially putting at risk both human lives and infrastructure (Figure 1.1). Not surprisingly, a lot of effort is put into understanding these systems, with studies aiming, for example, to predict where they will occur or to determine how far they travel. The focus of this thesis is on the latter, namely the transport of rocks under gravity. More specifically, I focus on the effect of fragmentation on the mobility, energy budget and dynamics of rock slides and rock falls.

The manner in which a rock mass travels down a slope is determined by several factors, such as size and geometry of the rock mass, the topography of the slope, as well as the material properties of both the transported material and substrate. Based on specific characteristics of the movement, different categories of rock movement can be defined. A common characterization system is the one suggested by Varnes (1978) and modified by Hungr et al. (2013). In this system, the separation of different groups is based on the type of material, the mode of failure and the dominant mode of transport. In terms of this system, three types are considered here: rock falls, rock slides and rock flows[1]. In general, rock falls can be defined as rock masses where the travel downslope is dominated by free falling, impacts and rolling, whereas rock slides are dominated by sliding. In contrast, flows are systems consisting of granular material, such that they flow and spread in a viscous manner. An example of a type of rock flow is the rock avalanches, which are produced when very large rock falls or slides are fragmented during transport, and are known to have exceptional long travel distances (Hsü, 1975). Specifically, in this thesis only dry systems are considered.

Fragmentation occurs readily in all of these systems, e.g. in the rock falls inevitable impact with the ground, or the rockslides travel over slope breaks. The process of fragmentation can be separated into two domains: instantaneous and continuous (Åström, 2006). In the former, the stresses that break the material apart are highly dynamic with numerous fractures propagating simultaneously. This type of fragmentation occurs typically during impacts of rock falls (Wang and Tonon, 2010). In the latter, the fragmentation occurs through grinding

[1]These can again be separated into subsets of these types; however, in the context of this thesis this rough separation is sufficient.

Figure 1.1: Landslides and rock slides triggered by the 2008 Wenchuan earthquake caused additional damage minutes after the earthquake. Photo by Martin Mergili

and communition of the material, typically seen in localized shear zones, for example, in faults or at the base of rock slides (Pollet and Schneider, 2004).

In general, the disintegration of a material causes loss of cohesion, which may change the further transport of the rock mass. Consider, for example, the case of an impacting rock fall. If no fragmentation occurs, the impact could be considered elastic[2], such that it would bounce up again, continuing as another free fall event. However, if fragmentation occurs, the material may, in all practical sense of time, be instantaneously transformed into a granular material. Any further travel by the rock mass would therefore follow the dynamics of a granular flow. This example illustrates one of the key difficulties in taking fragmentation into consideration: namely, that it can cause a transition from one type of rock movement to another: In the example above, from a rock fall to a rock flow.

Additionally, fragmentation consumes energy. How much energy is consumed is in general determined by the degree of fragmentation (Crosta et al., 2007). Knowledge of the degree of fragmentation before the event is, however, not readily available. Even if you were able to predict the degree of fragmentation, and from this determine the energy consumed by the fragmentation, it is not obvious how the energy budget of the system changes because it is

[2] A completely elastic impact is a theoretical end-member. Usually, one assumes a "non-elastic impact" by assuming the velocity after the impact to be lower, but proportional to the impact velocity. The proportionality constant is often called the coefficient of restitution and reflects the velocity lost during the impact (Dorren, 2003)

not known how the other energy dissipating terms (e.g. friction) is changed by the transition from a cohesive block to a granular flow. For example, Hsü (1975) proposed that fine-grained material can act to lubricate the rockslide, leading to a very low effective coefficient of friction. This, in turn, means that precise prediction of the mobility of fragmenting gravitational rock movements is difficult, if not impossible.

Perhaps due to their exceptional high mobility and highly fragmented deposits, most studies of fragmentation during gravitational rock movements focus on rock avalanches (Figure 1.2). These catastrophic rockslides are produced when very large (volume $> 10^6$ m^3) rockfalls or rockslides disintegrate during motion and travel downslope at high speeds (up to 150 km/h), reaching very long runout. The high mobility of rock avalanches is still one of the big unsolved problems in Geoscience, and several explanations have been suggested to explain it (e.g. Kent, 1966; Shreve, 1968; Hsü, 1975; Melosh, 1979; Campbell, 1989; Kilburn, 2001; Legros, 2002; Davies and McSaveney, 2009; Staron and Lajeunesse, 2009). Because the deposits of rock avalanches are highly fragmented, several authors have suggested that fragmentation can explain the high mobility, by, for example, a lubricating effect of fine-grained material (e.g. Kilburn, 2001; Pollet and Schneider, 2004) or a decreased normal stress at the base due to dispersive stresses from exploding fragments (e.g. Davies and McSaveney, 2009). However, none of the mechanisms proposed have been shown to be universally relevant. The fragmentation that takes place in a rock avalanche is generally recognized to occur by grinding and communition (Crosta et al., 2007). An exception is perhaps during the initial breakup of the material, when the quasi-intact rock mass can, for example, fragment by tensile fracture. Though the entire deposit show signs of fragmentation, most intense fragmentation is often observed in bands of localized strain, which is interpreted to take up most of the internal deformation (Pollet and Schneider, 2004).

The fragmentation of rock falls has also gained some recognition in the literature. Mostly this involves impact studies, where one evaluates the energy budget and the degree of fragmentation as a function of the impact velocity (e.g. Giacomini et al., 2009; Wang and Tonon, 2010). In an effort to model the consequences of a fragmenting rock fall, Frattini et al. (2012) implemented the current knowledge of impact fragmentation in a numerical model and compared the runout to those which assumed no fragmentation. From their models, they report that fragmentation did change the runout; however, they did not specify how.

Direct observations of gravitational rock movements at sufficient spatial and temporal resolution are rare. Modeling serves as a valuable tool to constrain the transport mechanisms, where direct observation is lacking. Additionally, by simplifying and isolating the governing processes, models provide a platform for understanding the complexity of nature[3]. In terms of transport models, fragmentation is a particular difficult problem to deal with (Figure 1.3). First of all, most models consider the material properties constant and assume either elastic blocks or cohesionless granular material. Any transition from one to the other is difficult, especially considering the computational power this would require. Secondly, due to computational costs or experimental limitations related to resolving all the relevant scales, most modelers would

[3]Someone once told me: a model containing all the complexity of nature is as useful as a 1:1 map

Figure 1.2: The Urdbøurdi, an example of a rock avalanche from Telemark, Norway. Photo by Terje Christiansen (www.flickr.com)

prefer not to explicitly model the fragmentation process, but rather use a simple relationship linking the initial conditions before the fragmentation event to the final products. For such a relationship to be useful, it must provide a fragment size distribution and the kinetic energies and directions of all the fragments after fragmentation has occurred. Unfortunately, such a relationship does not yet exist.

Based on the review above, it is safe to presume that little is known of how the process of fragmentation affects the transport of gravitational rock movement. It is the aim of this thesis to begin to uncover the most basic phenomena related to the fragmentation of gravitational rock movements. I do this, in perhaps the simplest way possible, by considering the oblique impact of a block, with fragmentation occurring self-consistently, and studying its following transport and emplacement. The specific questions I aim to answer in this thesis are: (1) Under what conditions does fragmentation occur and which parameters control it? (2) If more than one parameter, how are they related? (3) How does the mobility change with varying degree of fragmentation? (4) How is the energy budget affected? (5) What are the controlling parameters for the mobility and energy budget of gravitational rock movements?

In Chapter 2 the methods used in this thesis are presented, including the designing of the new analogue material and the experimental setup. The analogue material is designed to behave similar to natural rocks, i.e. it deforms in a brittle manner with limited elastic and ductile strains up to a certain critical stress, beyond which the material breaks and deforms irreversibly. Quantitative information from the experiments is achieved from image analysis,

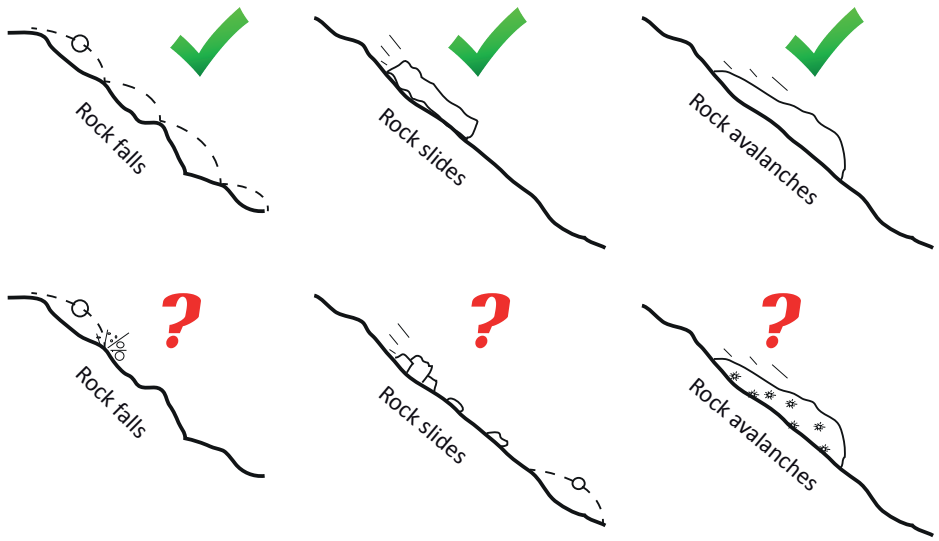

Figure 1.3: Illustrations of current models shortcomings relating to fragmentations: While they successfully can describe the ballistic path and impact of rock falls, the sliding block of a rock slide or the granular flow of a rock flow, they cannot take into consideration break-up of the material. The main reason for this is the change of material properties and dynamics, and the lack of a parameterization of the kinetics after a fragmentation event.

which provides the time evolution of several relevant factors such as area and velocity of the sample through the transport. Also presented in this chapter is a comparison between our experiments and the more typically used granular models, which reveal that the kinetics of a cohesionless granular material is very different from that of our models: where sand experiences both extension and compression during transport, a fragmenting block experiences only extension. This is found to have a profound effect on both the final area and the final position of the deposits.

In Chapter 3 the relevant parameters for fragmenting gravitational rock movements are derived by dimensional analysis and their role in the gravitational transport of rocks is studied through a parameter study. In particular, the basal friction, material strength and aspect ratio of the samples is considered. This study shows that fragmentation consumes energy, causing the reduction of the center of mass' travel distance. However, it also shows that the fragmentation allows the material to spread, such that the front travels further with increasing degree of fragmentation. The estimated energy consumed by fragmentation is found to be well described by a logarithmic curve, with as much as 25 % of the potential energy consumed by fragmentation.

The parameter study presented in Chapter 3 show that both the material strength and the aspect ratio of the sample controls the degree of fragmentation. In Chapter 4, an analytical model is considered that relates these two variables, as well as the fall height and topography,

to the degree of fragmentation, such that the latter can be expressed as a function of one parameter (S_{eff}). The parameter is derived by considering the peak tensile stress in an elastic plate estimated from the elastic thin plate theory modified by a factor accounting for the samples thickness. Low values of S_{eff} reflect a sample under conditions that is insufficient to break it, an intermediate value of S_{eff} reflects a sample that may fragment but only break apart into a few pieces, a high value of S_{eff} reflects a sample that will undergo severe fragmentation – approaching a granular material. This parameter can therefore be used to predict the degree of fragment solely from initial and boundary conditions. Further, the dominant mode of transport of a system depends on the degree of fragmentation, e.g. a highly fragmented material can be considered a granular flow while an intact rock mass is considered a sliding block. The value of S_{eff} may therefore help to determine the most likely mode of transport of a rockslide yet to occur. To verify its applicability, the value of S_{eff} is calculated for the Seymareh rock avalanche in Iran. The value correctly reflects a system within the highly fragmented regime.

Finally, in Chapter 5 the experimental models are compared to a natural data set of nine rock avalanches. The comparison reveals a good match between the experimental results and the natural rock avalanches. This therefore suggests that fragmentation is a governing process in the transport of rock avalanches.

Each of the following chapters in this thesis is written as an individual manuscript, and is either published, submitted or ready for submission to scientific journals.

References

J. A. Åström. Statistical models of brittle fragmentation. *Advances in Physics*, 55(3-4): 247–278, May 2006. doi: 10.1080/00018730600731907.

C. S. Campbell. Self-lubrication for long runout landslides. *The Journal of Geology*, 97 (6):653–665, 1989. URL `http://www.jstor.org/stable/10.2307/30062196`.

G. B. Crosta, P. Frattini, and N. Fusi. Fragmentation in the Val Pola rock avalanche, Italian Alps. *Journal of Geophysical Research*, 112:F01006, February 2007. doi: 10.1029/2005JF000455.

T. R. Davies and M. J. McSaveney. The role of rock fragmentation in the motion of large landslides. *Engineering Geology*, 109(1-2):67–79, 2009.

Luuk K. a. Dorren. A review of rockfall mechanics and modelling approaches. *Progress in Physical Geography*, 27(1):69–87, March 2003. ISSN 14770296. doi: 10.1191/0309133303pp359ra. URL `http://ppg.sagepub.com/cgi/doi/10.1191/0309133303pp359ra`.

P. Frattini, G. B. Crosta, and F. Agliardi. Rockfall characterization and modeling. In *Landslides - Types, Mechanisms and modelling*, pages 267–281, 2012. ISBN 9780511740367.

A. Giacomini, O. Buzzi, B. Renard, and G.P. Giani. Experimental studies on fragmentation of rock falls on impact with rock surfaces. *International Journal of Rock Mechanics and Mining Sciences*, 46(4):708–715, June 2009. doi: 10.1016/j.ijrmms.2008.09.007.

K. J. Hsü. Catastrophic debris streams (sturzstroms) generated by rockfalls. *Geological Society of America Bulletin*, 86(50117):129–140, 1975. URL `http://bulletin.geoscienceworld.org/content/86/1/129.short`.

O. Hungr, S. Leroueil, and L. Picarelli. The Varnes classification of landslide types, an update. *Landslides*, 11(2):167–194, November 2013. doi: 10.1007/s10346-013-0436-y.

P. E. Kent. The transport mechanism in catastrophic rock falls. *The Journal of Geology*, 74(1):79–83, 1966. URL `http://www.jstor.org/stable/10.2307/30075179`.

C. R. J. Kilburn. *The flow of giant rock landslides*. Elsevier B.V., 2001. ISBN 0444505601.

F. Legros. The mobility of long-runout landslides. *Engineering Geology*, 63 (3):301–331, 2002. URL http://www.sciencedirect.com/science/article/pii/S0013795201000904.

H. J. Melosh. Acoustic Fluidization : A New Geologic Process? *Journal of Geophysical Research*, 84(9):7513–7520, 1979.

N. Pollet and J. -L. M. Schneider. Dynamic disintegration processes accompanying transport of the Holocene Flims sturzstrom (Swiss Alps). *Earth and Planetary Science Letters*, 221(1-4):433–448, April 2004. doi: 10.1016/S0012-821X(04)00071-8.

R. L. Shreve. Leakage and fluidization in air-layer lubricated avalanches. *Geological Society of America Bulletin*, 79(5):653–658, 1968. doi: 10.1130/0016-7606(1968)79. URL http://bulletin.geoscienceworld.org/content/79/5/653.short.

L. Staron and E. Lajeunesse. Understanding how volume affects the mobility of dry debris flows. *Geophysical Research Letters*, 36(12):2–5, June 2009. ISSN 0094-8276. doi: 10.1029/2009GL038229. URL http://www.agu.org/pubs/crossref/2009/2009GL038229.shtml.

D. J. Varnes. Slope movement types and processes. *Transportation Research Board Special Report*, 1978.

Y. Wang and F. Tonon. Discrete Element Modeling of Rock Fragmentation upon Impact in Rock Fall Analysis. *Rock Mechanics and Rock Engineering*, 44(1):23–35, July 2010. ISSN 0723-2632. doi: 10.1007/s00603-010-0110-9.

Chapter 2

Modelling Fragmentation in Rock Avalanches

This article is removed from the online version but is available for download from
http://dx.doi.org/10.1007/978-3-319-05050-8_16

Ø. T. Haug, M. Rosenau, K. Leever, O. Oncken

Published in *Landslide Science for a Safer Geo-Environment* (2014), doi:10.1007/978-3-319-05050-8 16

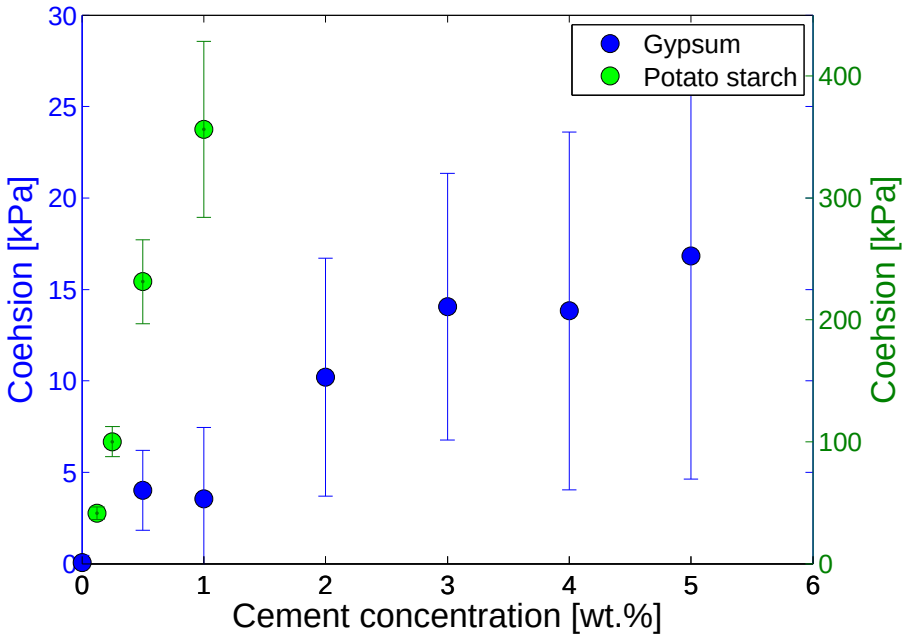

Figure 2.8: Cohesion of analogue material as a function of the cement concentration: Cohesion of the samples using gypsum-cement (blue) can be read from the left axis, and the cohesion from potato starch-cement (green) from the right.

2.7 Cohesion: additional material testing after publication

After publication of this article, further material testing was performed using triaxial tests. Unlike the uniaxial tests reported above, these tests include a finite confining pressure, i.e. non-zero σ_2 and σ_3. The tests was performed with $\sigma_2 = \sigma_3 = 0, 50, 100, 150$ mbar. Plotting the normal stresses at failure against the corresponding shear stresses allows for the determination of the cohesion from the intersecting line from a linear regression on the shear axis. The result from this analysis is presented in Figure 2.8.

The cohesion is, unlike the shear strength, determined from a large number of tests over a range of confining pressures. This therefore provide better constraints on the material strength than the shear strength.

Chapter 3

Effect of Fragmentation on the Mobility of Gravitational Mass Movements: Insights from Analogue Experiments

Abstract

The mobility of gravitational rock movements can be difficult to predict due to complex interactions of numerous physical processes, such as fragmentation of the rock mass and its effect on the energy dissipation of basal and internal friction. Gravitational mass movements are typically modeled as movements of rigid bodies or granular flows. However, there exists a wide spectrum of brittle, fragmenting bodies in between these end-members which are not captured by existing models. Here, we present a model aimed at closing that gap: a quantitative description of the mobility of fragmenting masses. Using dimensional analysis, we derive a set of dimensionless parameters that characterize the role of fragmentation in rock falls and rock slides. Taking advantage of a newly developed rock analogue material, we perform a total of 109 experiments to study the effect of fragmentation on the mobility and energy budget of gravitational rock movements. Our results show that the travel length of the center of mass decreases with the degree of fragmentation. In contrast, the area and the runout of the front of the deposits increase with a higher amount of fragmentation. The energy consumed by fragmentation increases with the degree of fragmentation and follows a logarithmic curve, with values of fragmentation energy ranging from 0 % to ≈ 25 % of the potential energy. Despite the energy consumption by fragmentation, an increased degree of fragmentation causes a larger amount of spreading of the material, causing an increased mobility.

Keywords
Rock slides, Rock Falls, Fragmentation, Analogue material, Analogue modeling

Ø. T. Haug, M. Rosenau, K. Leever, O. Oncken

Submitted to *Journal of Geophysical Research*

3.1 Introduction

Rock falls, rock slides and rock avalanches can have high and unpredictable mobility, which makes the assessment of the hazard associated with them difficult. Of the factors that can influence the mobility of rock movements, fragmentation has received little attention, despite its occurrence in all types of gravitational rock movements for a wide range of sizes. The process of fragmentation is known to consume energy (*Locat et al.*, 2006; *Crosta et al.*, 2007), which should ultimately reduce the mobility of the movements. Nevertheless, several studies suggest that fragmentation may lead to an increase of the mobility of rock avalanches (*Pollet and Schneider*, 2004; *Davies and McSaveney*, 2009; *Bowman et al.*, 2012). This suggests a complex interplay between the fragmentation process and the other energy-dissipative processes (e.g. friction), which is not yet understood.

The lack of understanding stems mainly from the lack of observations: the process of fragmentation is rarely directly observed as it occurs in nature. The current approach is, therefore, to infer kinematic and dynamic properties *a posteriori* from the deposits (e.g. *Pollet and Schneider* (2004); *Locat et al.* (2006); *Crosta et al.* (2007)). This approach suffers from a large number of assumptions and simplifications. Recently, seismological monitoring has captured active gravitational mass movements (*Deparis et al.*, 2008; *Dammeier et al.*, 2011), thereby opening for a more direct quantitative measure of rock movement kinematics and dynamics. However, to harvest the full potential of these observations, we need a good understanding of the processes at work in the movements. For example, how much does the energy transferred to the ground depend on the fragmentation of a rock mass?

Models of gravitational rock movements often assume rigid or elastic particles, either as individual particles (e.g. rock fall models of *Agliardi and Crosta* (2003)), or as a collection of particles in a granular material (e.g. rock avalanche models of *Davies and McSaveney* (1999); *Manzella and Labiouse* (2012)). Fragmentation, or any reduction of particles sizes during motion, is largely neglected. Important exceptions are the analogue models of *Bowman et al.* (2012), which showed that experimental samples accelerated after fragmentation, causing fragmenting samples to travel farther than pre-fragmented ones.

The role the process of fragmentation plays in gravitational rock movements is still largely unknown, and several questions remain unanswered: (1) what controls the degree of fragmentation? (2) How is the mobility of gravitational rock movements affected by the process of fragmentation? (3) How is the energy budget changed? Here, we use lab-scale models of fragmenting gravitational mass movements that allow us to simulate the process of fragmentation under controlled conditions, monitor kinematics of fragmenting gravitational mass movements at high temporal resolution, and to estimate their energy budgets. Taking advantage of a newly developed rock analogue material (*Haug et al.*, 2014), the cohesion of which can be conveniently controlled over 3 orders of magnitude, we perform a total of 109 experiments. This ensures statistically reliable results over a wide range of degree of fragmentations. Notice though, our models do not aim to reproduce the full complexity of natural gravitational mass movement, they are far too simple for that. Rather, we aim to study the mobility and behavior of a simple sliding system where fragmentation occurs

self-consistently.

In Section 3.2, we give a brief overview of fragmentation in the framework of gravitational mass movements, as it is presented in the current literature. We then identify fundamental parameters of the processes by means of dimensional analysis (Section 3.3). Our new experimental setup, as presented in section 3.4, has been designed such that these parameters can be controlled and monitored. The experiments illustrate how fragmentation consumes energy as a function of degree of fragmentation, but at the same time promotes spreading of the material, which causes a larger area of the deposits and a longer reach of the front of the deposit. (section 3.5). The results of our experiments suggest that fragmentation in gravitational rock movements leads to increased mobility, despite the observation that energy is lost to fragmentation (section 3.6).

3.2 Fragmentation in gravitational rock movements

The dominating mechanism behind the fragmentation process differs depending on the type of gravitational rock movement. In the case of rock falls, the rocks impact the ground after a period of free fall. One may therefore assume that this causes dynamic stresses that lead to an instantaneous type of fragmentation (*Åström*, 2006). In such systems, the degree of fragmentation is known to depend on the velocity of the impact, angle of the impact, properties of the ground, as well as the initial fracture network. In particular, fragmentation does not occur below specific values of these parameters (*Wang and Tonon*, 2010), suggesting that there exists a threshold for fragmentation. In the case of impact velocity, this threshold may be related to a continuous phase transition (*Kun and Herrmann*, 1999), where impacts below a critical velocity result in a damaged state characterized by the largest fragment being approximately of the same size as the initial sample. Impacts at velocities higher than the critical velocity result in a fragmented state, characterized by the largest fragment being much smaller than the initial sample (*Kun and Herrmann*, 1999; *Timár et al.*, 2012). It is, however, unclear how this phase transition is reflected by the mobility and energy budget of rock falls.

Fragmentation in rock falls is difficult to model, and numerical models of rock falls largely ignore fragmentation (*Wang and Tonon*, 2010). Instead, one often applies a coefficient of restitution that deals with both the energy lost from the impact with the ground, and the energy consumed by the fragmentation process (*Agliardi and Crosta*, 2003). While such models have been successful at predicting rock fall runout, comparisons between rock fall models and field tests have shown that fragmentation of rocks can cause fragments to have higher velocity than that predicted by the model (*Agliardi and Crosta*, 2003). Such increase in mobility cannot be explained using an effective energy loss at impact.

For rock falls and rock slides with volumes larger than $\sim 10^5\ m^3$, the motion can transform the quasi-solid material into rock avalanches (*Kilburn*, 2001). The deposits of the latter consist of highly fragmented material. Often, one separates the fragmentation of these system into two parts (*Pollet and Schneider*, 2004). (1) A primary (static) fragmentation, where the rock mass breaks apart along pre-existing fractures into fragments of more competent rock, and (2)

Variable	Form	Model	Nature
$\mathcal{L}$	L/l	$4-12$	$10^{-2}-10^{2}$
$\mathcal{H}$	H/l	4.7	$10^{-3}-10^{3}$
$\mathfrak{a}$	l/h	$2.05-30.0$	$10^{-2}-10^{3}$
$\mathcal{A}$	$A/V^{2/3}$	$4-60$	$1-60$
m_c	M/m_{max}	$1.05-19.5$	1–??
$\mathcal{F}$	$\rho g H/C$	$3.0\cdot10^{-2}-2.7$	$10^{-4}-10^{1}$
μ		$0.2-0.55$	??
θ		45°	$0^\circ-90^\circ$
ϕ		30°	??

Table 3.1: List of the dimensionless parameters and their values in the models and nature

a dynamic fragmentation where these particles are continuously reduced in size by grinding and comminution (*Pollet and Schneider*, 2004; *Imre et al.*, 2010).

Many studies that look at the effect of fragmentation in rock avalanches estimate the amount of energy spent on fragmentation (*Crosta et al.*, 2007; *Locat et al.*, 2006). In general, these studies suggest that as much as 30 % of the potential energy can go into fragmentation. This energy is consumed at the cost of the kinetic energy, and should ultimately lead to a shorter runout. However, *Bowman et al.* (2012) show in their models that material accelerates after a fragmentation event, causing a longer runout the higher the degree of fragmentation. The mechanism that can lead to such acceleration is still not understood, and further testing is needed to establish the energy budget of fragmenting rock slides.

3.3 Dimensional Analysis and Scaling

When developing a method for testing the effects of fragmentation, we must first understand which variables are relevant and how they are related. Dimensional analysis is a powerful tool to gain such insights. The method of dimensional analysis is described in detail by *Barenblatt* (2003). The general procedure is to list up all relevant parameters in the model and define a set of dimensionless parameters that characterize the system.

In Figure 3.1 the relevant geometrical and kinematic variables in our model are illustrated. The sketch shows a cuboid shaped sample of mass M with height h and length l elevated to a height H on a slope at angle θ. Once released, the sample will first slide down the slope, after which it obliquely impacts and turns around onto the horizontal plate. If fragmentation occurs, it is at this point. One of the key observables in our model is the travel distance, L, of the sample, which is defined as the horizontal distance between the sample's center of mass at its starting point and at its final position (see Figure 3.1). Also measured in our

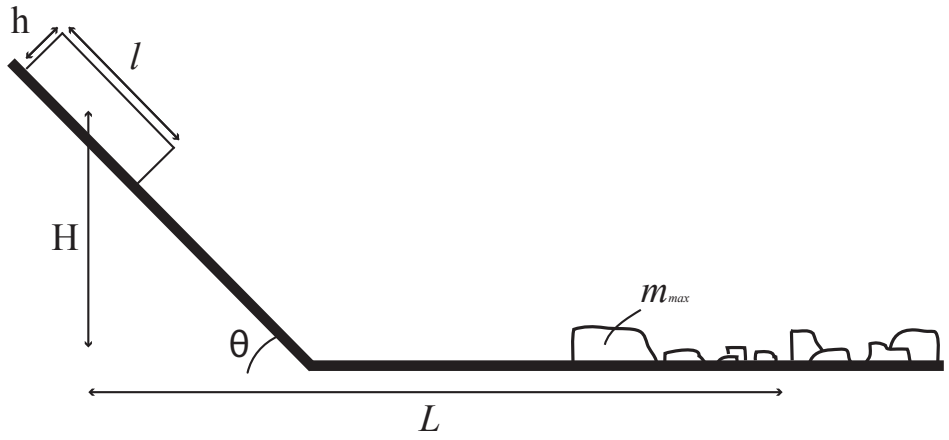

Figure 3.1: Sketch of the geometrical and kinematic variables considered in the model

models is the runout, L_f, which is defined as the horizontal distance of the sample's initial front position and the front of the final deposits. However, as the center of mass is the relevant parameter for studying the energy budget of the system, the runout is not treated explicitly in the dimensional analysis. Another parameter of interest is the final area of the deposits A, defined as the total surface area covered by the material. As the material impacts and moves onto the horizontal plate fragmentation is resisted by its cohesion. The cohesion C of the sample is, therefore, included in the analysis. Similar to *Timár et al.* (2012), we characterize the amount of damage the material experiences by the mass of the largest fragment, m_{max}. Finally, the gravitational acceleration, g, the coefficient of friction between the material and the base plate, μ, and the angle of internal friction, ϕ, are included.

Altogether, we have a list of 12 parameters (L, H, h, l, A, θ, C, M, m_{max}, g, μ and ϕ). There are 3 fundamental units in this list: mass, length and time. Buckingham's Pi theorem (*Barenblatt*, 2003) states that we need 12 - 3 = 9 dimensionless parameters to characterize the system.

The first parameter is the relative travel distance

$$\mathcal{L} = \frac{L}{l} \tag{3.1}$$

which is the ratio between the travel distance and the size of the sample. The second parameter is the relative fall height

$$\mathcal{H} = \frac{H}{l} \tag{3.2}$$

The third parameter defines the geometry of the sample

$$\mathfrak{a} = \frac{l}{h} \tag{3.3}$$

and is the aspect ratio of the sample. The aspect ratio takes values from 0 to ∞: a value of 0 represents upright 2D rectangle, a value of 1 represents a perfect cube and a value of ∞ represents a 2D rectangle lying down on its flat side.

The fourth parameter is the dimensionless area of the deposits

$$\mathcal{A} = \frac{A}{(hl^2)^{2/3}} = \frac{A}{V^{2/3}} \tag{3.4}$$

which reflects the area of the deposits relative to the initial volume of the sample. This normalization was also used by (*Davies and McSaveney*, 1999) and *Bowman et al.* (2012).

The non-dimensionalization of m_{max} gives

$$m_c = \frac{M}{m_{max}} \tag{3.5}$$

This is the inverse of the parameter that was suggested by *Kun and Herrmann* (1999) as the order parameter for the phase transition between the damaged and the fragmented state. It has also been used by *Nocilla et al.* (2009), to characterize the degree of fragmentation of rock falls. In general, m_c provides a measure for the damage the material has experienced and takes values from 1 to ∞, where a value of 1 reflects a completely intact sample, while an increasing value reflects an increasingly fragmented sample.

The next variable to consider is the strength of the material

$$\mathcal{F} = \frac{\rho g H}{C} \tag{3.6}$$

which is the ratio between the specific potential energy and the cohesion, i.e. the ratio between the energy available and the resistance to fragmentation. For systems where $\mathcal{F} \ll 1$, cohesion dominates, suggesting that the material will not fail, whereas for $\mathcal{F} \gg 1$, the potential energy dominates and fragmentation may occur. This is the same parameter that was suggested by *Locat et al.* (2006) to determine the degree of fragmentation for natural rock avalanches.

Finally, the last three dimensionless parameters are the angle of the plane, θ, the coefficient of basal friction, μ, and the angle of internal friction, ϕ, which are already dimensionless.

3.3.1 The values of the dimensionless parameters

For our models to be comparable with natural systems, the values of the dimensionless parameters given above ($\mathcal{L}$, $\mathcal{H}$, $\mathfrak{a}$, $\mathcal{A}$, m_c, $\mathcal{F}$, θ, μ, ϕ) must be similar to those found in nature. The values from the scaling analysis are summarized in Table 3.1.

The value of $\mathcal{L}$, which relates the travel distance to the length of the sample, varies a lot in nature. In the case of rock falls, the length, l, can in principle be of any size (*Varnes*, 1978), but typically varies between 10^{-1} to 50 m (converted from the volumes of rock falls given in *Agliardi and Crosta* (2003)). Assuming that the travel distances for rock falls are between 10^{-1} to 10^{1} m, values of $\mathcal{L}$ for rock falls range between 10^{-2} to 10^{2}. For rock slides, we assume a typical length of 10^{0} to 10^{2} m, and a travel distance of 10^{1} to 10^{2} m, giving a range of $\mathcal{L}$

between 10^{-2} and 10^{1}. For rock avalanches, the length typically varies from 10^{1} to 10^{3} m and travel distances in the range of 10^{2} to 10^{3} m (*Lucas et al.*, 2014), so that $\mathcal{L}$ ranges between 10^{-2} to 10^{1}.

The fall height of gravitational rock movements is assumed to range from 10^{0} to 10^{3}. This gives a possible range of the relative fall height, $\mathcal{H}$, of 10^{-3} to 10^{3}. The fall height is not varied in our experiments, and has a constant value of 4.7.

The thicknesses, h, of rock falls are assumed to range from 10^{-1} to 10^{1} m; consequently, aspect ratios of rock falls range between 10^{-2} and 10^{2}. For slides, the thickness is assumed to vary from 10^{-1} to 10^{1} m, giving a range of $\mathfrak{a}$ from 10^{-1} to 10^{3}. For rock avalanches, aspect ratios range from 1 to 20 (*Lucas et al.*, 2014). In our experiments, $\mathfrak{a}$ is varied from 2.05 to 30.0, i.e. we only consider situations where the sample is a flat cuboid.

The lowest value possible for the normalized area ($\mathcal{A}$) occurs for no change of area, assuming no contraction is possible. In case of a cuboid slide, this situation would give a value of $\mathcal{A} = (h/l)^{2/3} = \mathfrak{a}^{2/3}$, i.e. varying from 1 to 130 for the values given for rock avalanches. However, if spreading of the material occurs, data collected from *Locat et al.* (2006) gives $\mathcal{A}$ up to 60. The values of $\mathcal{A}$ for our experiments range from 4 to 60.

The damage experienced by the sample is here measured by $m_c = M/m_{max}$. Thus, for any system, $m_c \geq 1$. The most fragmented systems found in nature are probably rock avalanches, with $m_c \gg 1$. The value of m_c varies in our experiments from 1.05 to 19.5, such that our models are systems of low to moderate degrees of fragmentation.

The bulk strengths of weathered and fractured rocks, as well as soil, are difficult to quantify. We model the gravitationally moving masses as homogeneous and isotropic material, with an effective strength characterized by bulk cohesion. The cohesion of competent rocks is of the order of 10^{6} to 10^{8} Pa (*Schellart*, 2000). Assuming a density of 2500 kg/m^3, we estimate that $\mathcal{F}$ in natural systems ranges from 10^{-4} to 10^{1}, i.e. from the cohesion-dominated to slightly dominated by potential energy. However, rocks in gravitational rock movements rarely consist of a uniform competent rock, and the value of $\mathcal{F}$ is expected to range also to higher values. In our experiments, the cohesion is varied from 3.5 ± 2.2 to 360 ± 72 kPa. The density is $1.6 \cdot 10^{3}$ kg/m^3. This gives $\mathcal{F} = 3.0 \cdot 10^{-2} - 2.7$, i.e. within the range seen for natural systems.

In the experiments, the coefficient of basal friction is varied between 0.2 and 0.55. The angle of the slope in the experiments and the angle of internal friction (θ and ϕ) are held constant at 45° and 30°, respectively.

3.4 Experimental Setup and Quantification of the Experiments

The experiments are performed by releasing a cuboid sample made of rock analogue material down a slope of 45° (Figure 3.2). At the base of the slope, the material impacts onto a horizontal plate, undergoes fragmentation, and finally comes to rest.

The analogue material is produced by mixing a well sorted fluvial sand (average grain size $\sim 300\mu m$) with either gypsum powder or potato starch, while both materials are dry. Then, $\sim$10 wt% water is added to the mixture and thoroughly stirred, to obtain a homogeneous

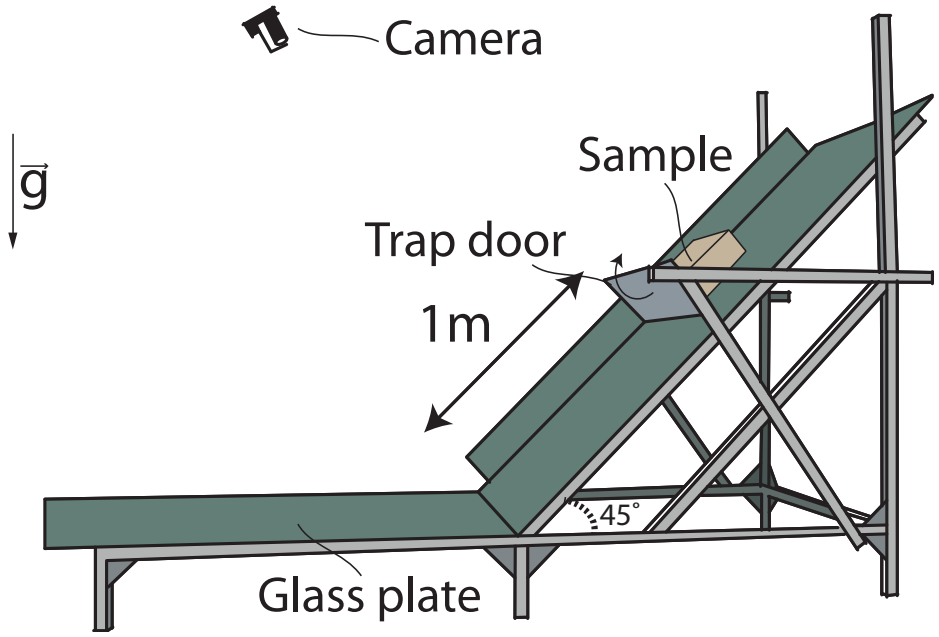

Figure 3.2: Drawing of the experimental setup

mixture. The material is left to set for 2 days (gypsum) or dried in a 900 W microwave oven for 15 minutes (potato starch). Properties of the analogue material have been determined by triaxial and ring shear tests (*Haug et al.*, 2014). The cohesion of the material is controlled by the amount of cementing agent added, with cohesion spanning 3 orders of magnitude: ranging from 3.5 ± 2.2 to 360 ± 72 kPa. The angle of internal friction is $\phi = 30°$ and the density, ρ, of the material is $1.6 \cdot 10^3\ kg/m^3$.

The experiments are monitored using two digital optical cameras: one camera captures the kinematics of the models at a frequency of 50 Hz (giving typically ~ 75 images for a ~ 1.5 second experiment), while the other takes a high spatial resolution (pixel length $\approx 500\mu$m, giving $\sim 2-3$ sand grains per pixel) still image of the final deposit. This ensures us both good temporal and spatial resolution of the results.

To obtain quantitative results from the experiments, the images from the two cameras are converted into binary form: pixels occupied by fragments are given value 1, while others are set to 0. Each isolated region of 1's in the binary image is considered a fragment, and its size is determined based on the number of pixels occupied by it. Fragments with an area lower than 10 pixels ($2.2 \cdot 10^{-6}\ m^2$) are considered to be background (i.e. their pixels set to 0) since they cannot be properly resolved. The volumes of the fragments are assumed to depend on their areas, which are estimated from their equivalent diameters, given by

$$d_{eq,i} = \sqrt{\frac{4A_i}{\pi}} \tag{3.7}$$

where A_i is the area of fragment i. If $d_{eq,i} < h$, where h is the thickness of the sample, the shape of a fragment is approximated by a sphere, and the volume is given by $V_i = \frac{4}{3}\pi(0.5d_{eq,i})^3$. If $d_{eq,i} \geq h$, the volume is estimated to be $V_i = A_i h$. The mass is calculated as $m_i = V_i \rho$.

To find the center of mass we use

$$\mathbf{R} = \frac{1}{M}\sum^{N} m_i \mathbf{r_i} \tag{3.8}$$

where $\mathbf{R} = (x_{cm}, y_{cm})$ is the center of mass, M is the total mass of the sample, N is the number of fragments and $\mathbf{r_i} = (x_i, y_i)$ is the position of each fragment where the x_i and y_i are the coordinates along the width and length of the plate, respectively. The travel length of the center of mass is determined by $L = y_{cm} - y_0$, where y_0 is the initial position of the center of mass.

The area of the deposits is determined by the area covered by any material, be it sand or cohesive fragments. The front of the deposits is determined in our experiments by the travel distance of the longest traveling fragment with a mass larger than 1 % of the total mass of the sample.

Here, we report on three experimental series where the effect of fragmentation on the travel distance is tested: $\mathfrak{a}$-series, $\mathcal{F}$-series and μ-series. In the first two series, the base plates are made of glass with friction against the sample (i.e. basal friction) of $\mu = 0.2$. While this coefficient of friction might be considered much lower than what is expected in nature, we choose this because it increases the spreading of the fragmented material and detection of the fragments is easier. The effect of a higher friction is tested in the μ-series. The range of tested values is shown in Table 3.1. (1) In the $\mathfrak{a}$-series, the aspect ratio of the sliding material ($\mathfrak{a}$) is systematically varied, while $\mathcal{F}$ is kept constant at 0.74. The aspect ratio was varied by varying the thickness (h) of the sample, while keeping the samples' length (l_0) constant at 0.15 m. (2) In the $\mathcal{F}$-series, the ratio between potential energy and cohesion is varied by systematically varying the cohesion of the samples. In this series of experiments, the aspect ratio is kept constant at 7.5. (3) In the μ-series, the cohesion is again varied, but this time the base on the horizontal plate is changed to a rubber mat, with a coefficient of friction of 0.55 with the sand. The plate on the slope in this series is also glass, ensuring the same impact velocity on the horizontal plate as in the other experiments.

3.5 Results

3.5.1 Observations

The evolution of a typical experiment can be seen in Figure 3.3. This figure shows that the material stays intact while sliding down the slope prior to the impact (Figure 3.3a). At impact (Figure 3.3b), the material breaks into several fragments with sizes ranging from the grain size of the sand up to a few centimeters. Closer observation of the fragmentation of the sample shows that the sample breaks apart in sequential events as it travels through the corner (Figure 3.3c). Fractures are observed to propagate in many directions, but failure

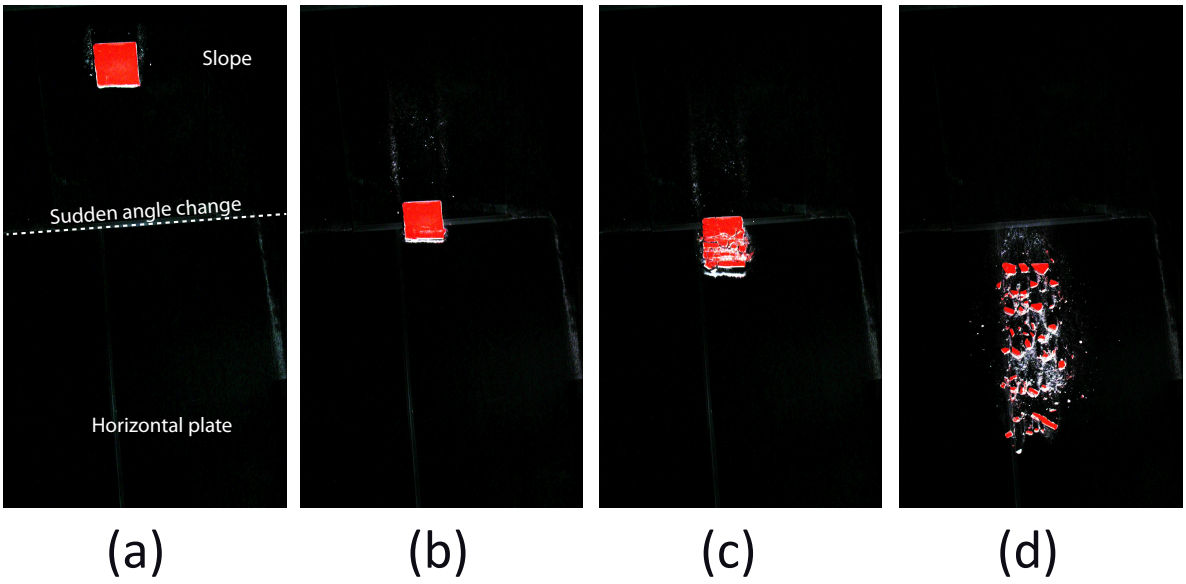

Figure 3.3: Sequential snapshots of an experiment with $\mathfrak{a} = 18.75$ and $\mathcal{F} = 0.74$. (a) 0.16 seconds before impact: the sample slides down the slope. (b) 0.02 seconds after impact: the sample fragment when impacting on the horizontal plate. (c) 0.04 seconds after impact: The fragmentation occurs in sequence with the sample's travel through the corner. (d) 0.32 seconds after impact: the fragments spread and slide on the horizontal plate.

appears to occur preferentially orthogonal to the direction of travel, recognized by a space between strips of fragments. The first event is recognized by a strip of fine-grained material (i.e. sand) traveling in front of the sample. The following events produce larger fragments, and break the sample apart in sequence with the sample's travel through the corner. After the sample has moved through the corner, the fragments slide and spread on the horizontal plane (Figure 3.3d) before coming to rest.

The velocities of the fragments on the horizontal plane show a gradient with respect to position: high velocities in the front and low in the back (Figure 3.4). Careful observations of the experiments (e.g. Figure 3.3) reveal that the fragments rarely move past each other, suggesting that the velocity gradient is not caused by segregation, i.e. by fragments with higher velocities moving to the front. Rather, it appears to be a direct consequence of the fragmentation process: the fragments from the first event of fragmentation have the highest velocity, the fragments from the second event have the second highest velocity, and so on. Also, an increase of the sizes of the fragments is observed from the front to the back (Figure 3.4), though fragments of all sizes are spread throughout the deposits.

The velocity of the front of the sample before, during and after impact is observed to be similar, suggesting that fragments have approximately constant velocity during fragmentation. Importantly, we do not observe any positive acceleration of the material.

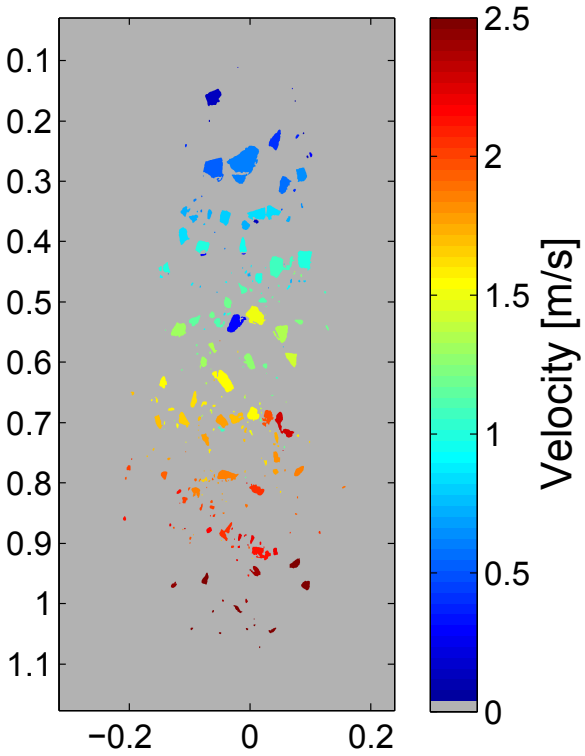

Figure 3.4: The velocity of fragments while they spread on the horizontal plate. A gradient is observed, with high velocity in the front and low in the back.

The degree of fragmentation (estimated by m_c) observed in the experiments for varying aspect ratios ($\mathfrak{a}$) and potential energy-to-cohesion ratios ($\mathcal{F}$) is plotted in Figure 3.5. Here, it is observed that m_c increases with both $\mathfrak{a}$ and $\mathcal{F}$. This shows the intuitive result that flatter cuboids experience a higher degree of fragmentation than more cubical shapes and that weaker material fragments more than stronger materials. This trend is, however, broken for the two points with largest $\mathfrak{a}$-value (colored white in Figure 3.5a). Several samples were prepared with these thicknesses (0.5 - 0.6 cm), but these data points represent the only two samples that did not fail while placing them onto the chute (before the experiment started). These two points therefore reflect the limit of reasonable $\mathfrak{a}$-values for our method, and they will not be considered in the further analysis.

The normalized area, $\mathcal{A}$, for the experimental slides is plotted against the degree of fragmentation in Figure 3.6. For both $\mathfrak{a}$ and $\mathcal{F}$-series, the areas are observed to increase as the degree of fragmentation increases. It is seen, that for $m_c > 5$, the data from the two experimental series plot along the same trend. In contrast, at m_c below 5, the points from the $\mathcal{F}$-series suddenly decrease to lower values.

In Figure 3.7, the travel distance of the samples' center of mass ($\mathcal{L}$) and the runout of

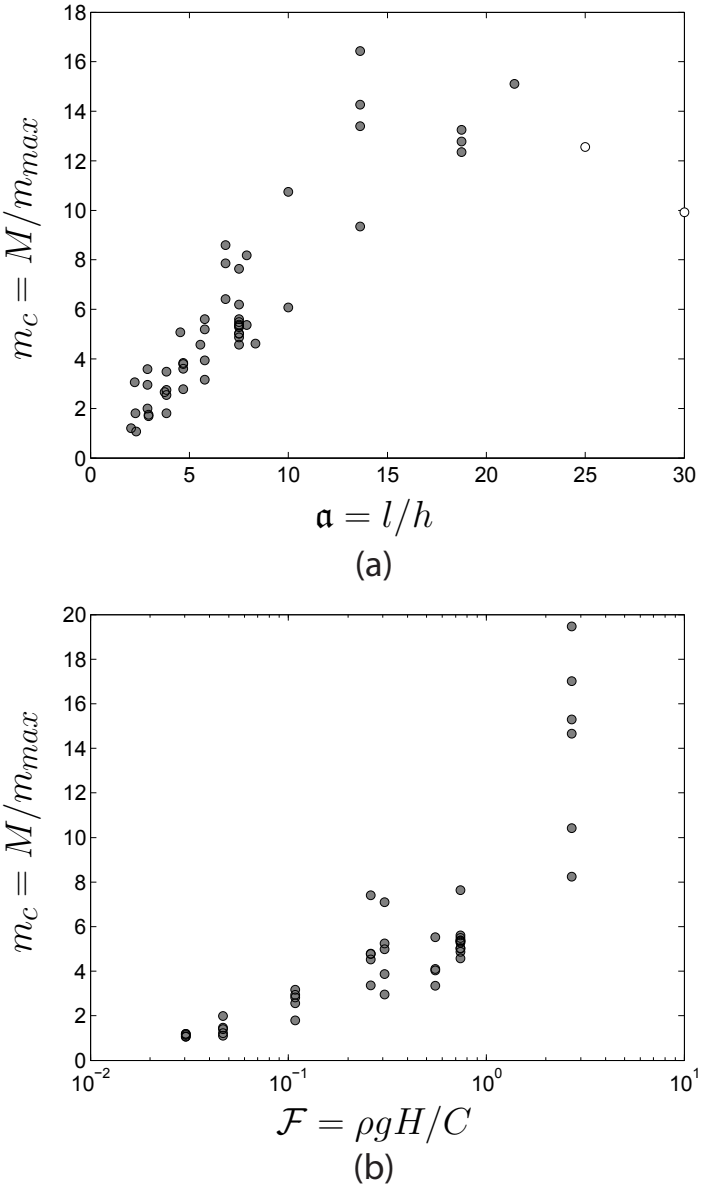

Figure 3.5: The degree of fragmentation, m_c, plotted against (a) the $\mathfrak{a}$-series with $\mathcal{F} = 0.74$ and (b) the $\mathcal{F}$-series with $\mathfrak{a} = 7.5$. The degree of fragmentation is observed to increase with both parameters.

the front of the deposits ($\mathcal{L}_f$) are plotted against the degree of fragmentation (m_c), for the three series of experiments. The travel distances from both $\mathfrak{a}$-series and $\mathcal{F}$-series are observed

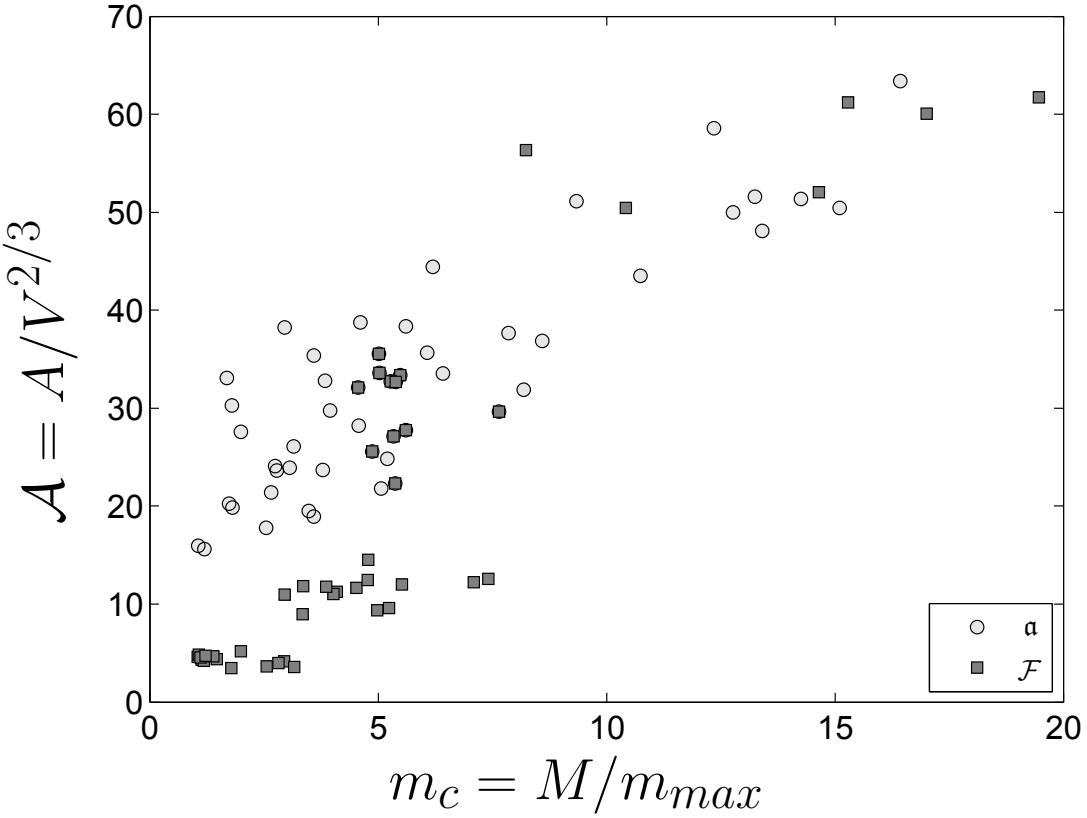

Figure 3.6: The relative area of the deposits plotted against the degree of fragmentation for the $\mathfrak{a}$ and $\mathcal{F}-$series. The relative area is seen to increase for both series, but a separation between the two series occur at $m_c \approx 5$.

to collapse onto one curve. The result from the μ-series plot below the other two series of experiments. For the $\mathfrak{a}$-series and $\mathcal{F}$-series, Figure 3.7a shows that as m_c increases, the travel distance decreases rapidly until a value of $m_c \approx 5 - 10$. As m_c increases above this, a decrease of travel distance is still observed, but the difference between experiments is less than for lower values of m_c. A similar trend is observed for μ-series, however, for samples that experienced little fragmentation (open squares), the travel distance is significantly lower than experiments with $m_c = 2 - 4$. A detailed study of the experimental images shows that these samples experience a strong deceleration at impact, suggesting these experiments represent a different impact mechanism than the other experiments. These points will therefore not be considered further in this study.

Unlike the center of mass, the distance traveled by the front of the samples for $\mathfrak{a}$ and $\mathcal{F}$-series show an increase with the degree of fragmentation (Figure 3.7b). Similar to the center

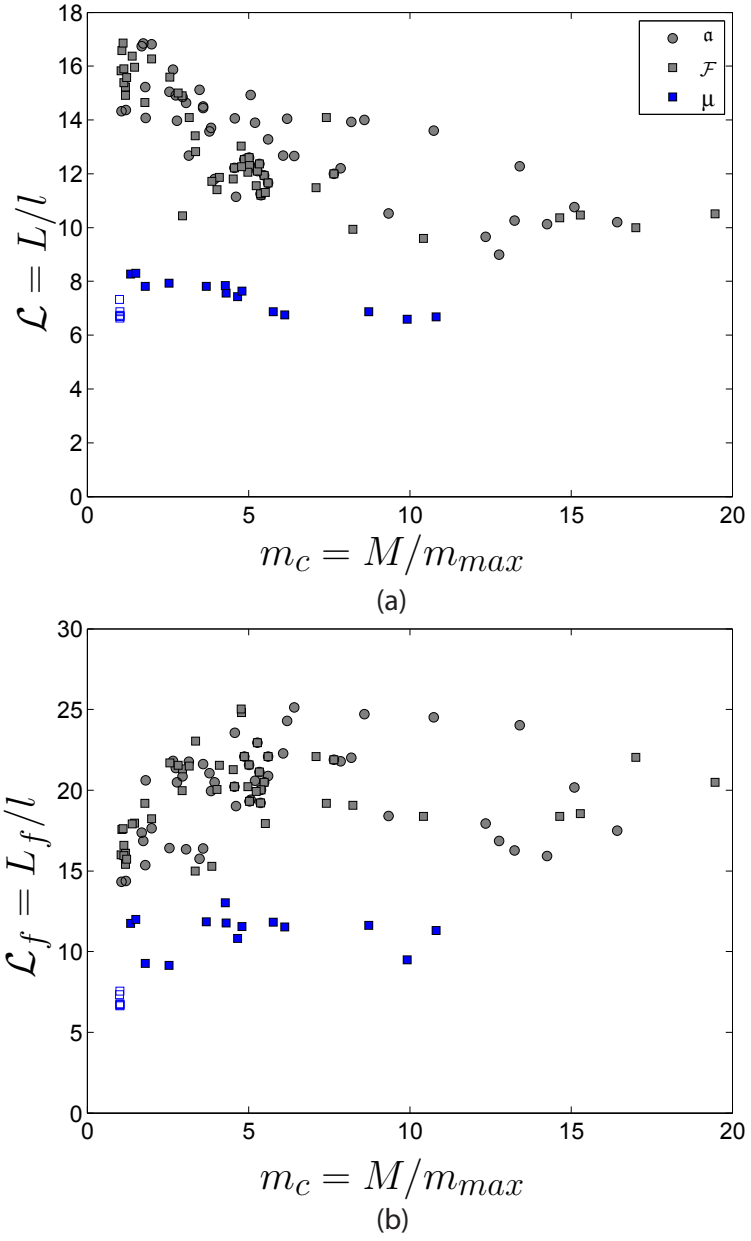

Figure 3.7: (a) The travel distance of the samples' center of mass plotted against the degree of fragmentation. A decrease in travel distance is observed with an increasing degree of fragmentation. (b) The displacement of the front of the deposits plotted against the degree of fragmentation. The front is observed to increase with the degree of fragmentation for $m_c < 5$, but for m_c above this level the front is seen to level off.

of mass, the front is also seen to be more strongly affected by the degree of fragmentation below $m_c \approx 5$. For degrees of fragmentation above this value, displacement of the front of the deposits is observed to saturate, or even decrease. The points showing the front of the deposits for μ-series do not show any clear relationship with m_c.

3.5.2 Determining the fragmentation energy

The results in Figure 3.7a demonstrate that the travel distance of the center of mass depends on the degree of fragmentation, where more fragmentation leads to shorter travel distances, suggesting an increased consumption of energy by fragmentation. In order to quantify this, we consider the conservation of energy of the system, which in general is given as

$$-\Delta E_p = \Delta E_k + W \tag{3.9}$$

where ΔE_p is the change of the potential energy, ΔE_k is the change of the kinetic energy and W is the work done on the system. The change of the potential energy is given by $\Delta E_p = MgH$. The velocity before and at the end of the experiment is zero, and $\Delta E_k = 0$. There may be several processes that contribute to the work term in Equation 3.9. Here, it is set to $W = W_\mu + W_i + W_f$, where W_μ is the Coulomb friction, W_i is the work done by the impact and W_f is the sum of work done by fragmentation and all other energy-consuming terms. Notice, this means we assume we can separate between the energy lost to the impact and that which goes into fragmentation.

Assuming that $W_f \approx 0$ when $m_c = 1$, we can solve Equation 3.9 for W_i,

$$W_i = Mg\left(H - \mu L_s\right)|_{m_c=1} \tag{3.10}$$

where L_s is the travel length of the samples center of mass along the travel path. We assume that W_i is constant for all experiments. This means that we consider any change of travel distance between a fragmenting and non-fragmenting experiment to be related to the fragmentation energy, and should therefore be included in W_f. Solving Equation 3.9 for W_f gives

$$W_f = Mg\left(H - \mu L_s\right) - W_i \tag{3.11}$$

where W_i is a constant given by Equation 3.10.

The fraction of potential energies consumed by the fragmentation for $\mathfrak{a}$-series and $\mathcal{F}$-series are plotted against the degrees of fragmentation in Figure 3.8. The data shows that for m_c between 1 to 5, W_f increases rapidly for increasing degrees of fragmentation. In experiments with degrees of fragmentation higher than 5, W_f seems to saturate as m_c increases. The results show that if $m_c > 5$ the fraction of potential energy consumed by fragmentation is between 20 % to 25 %.

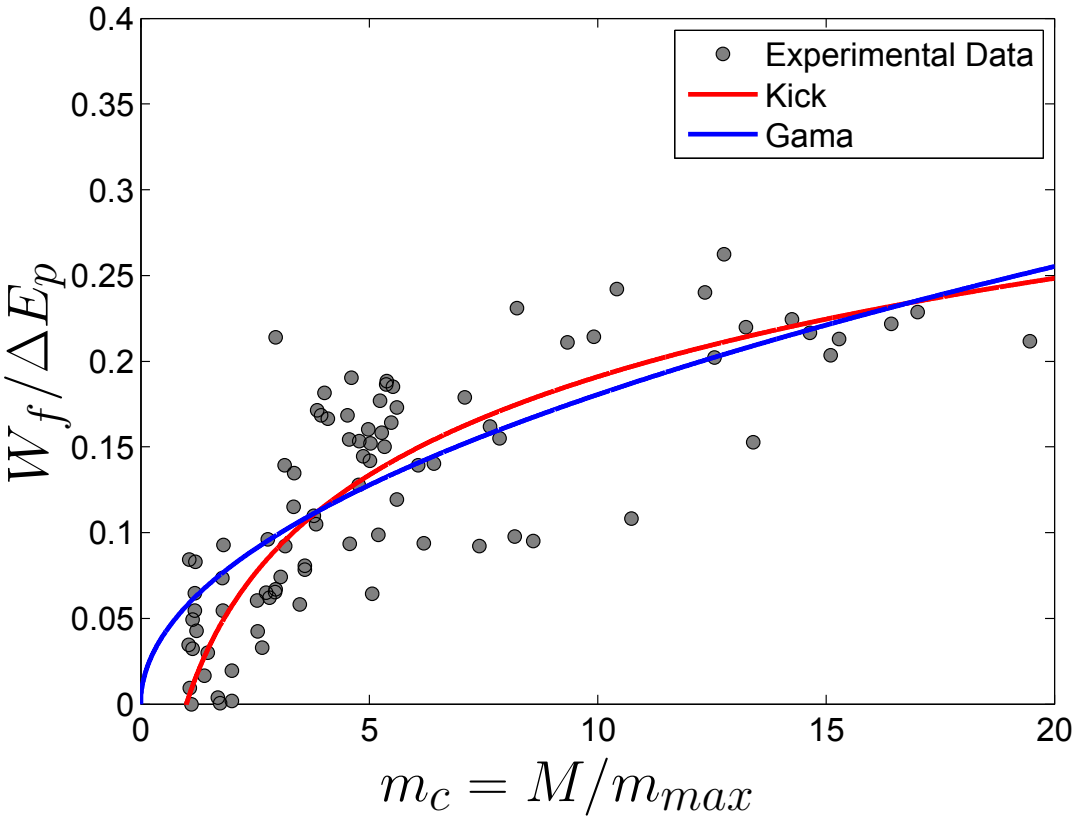

Figure 3.8: The fragmentation energy plotted against the degree of fragmentation. The fragmentation energy increase strongly for $m_c < 5$, but as m_c increase above 5 it appears to converge towards a value of 25 %.

3.6 Discussion

3.6.1 Interpretation of results

In the experiment presented in Figure 3.3, the fragmentation is observed to occur in sequential events. The images show that the sample breaks mainly orthogonally to the direction of travel. However, the first event appears different from the following ones from the size of the fragments produced: for the first event only fine material is observed while the later ones display fragments of a range of sizes. The first event is likely caused by the impact of the sample on the horizontal plate. In this respect, the sand observed in this event is probably caused by localized crushing, which occurs during the first impact. In the following events, the fragmentation appears to occur in a different manner. Considering the observation that thinner samples show a higher degree of fragmentation than thicker ones (Figure 3.5a), it is suggested

that these events occur due to elastic bending of the samples as they move through the corner. The fact that most fragments are produced in these events of fragmentation, suggests that elastic bending is the dominant mechanism for fragmentation in our experiments.

The velocity of the fragments in the front appears to remain nearly constant during the impact, such that, even after fragmentation has occurred, velocities of these fragments are high. This observation shows that one cannot simply assume an overall reduction of velocities of the fragments after a fragmentation event. Our results (Figure 3.4) show a range of velocities after fragmentation: from close to zero to the impact velocity of the sample. This observation may possibly explain the results obtained by *Agliardi and Crosta* (2003), when they compared their model to field tests and found that the velocity of some fragments were higher than what their models predicted. The consequence of the high velocity of these fragments is that fragments of the front travel much longer than the other fragments (Figure 3.7b), thereby causing a larger area of the deposits (Figure 3.6). This result shows how fragmentation, despite consuming energy, can increase the impact a gravitational rock movement can have on a site.

The normalized area of the deposits is seen to increase with the degree of fragmentation for both the $\mathfrak{a}$ and $\mathcal{F}$-series (Figure 3.6). This is caused by the increased amount of spreading, as the degree of fragmentation increases. However, the results from the two series differ from each other for values of m_c below ≈ 5. Comparing the experimental images from these experiments reveals that experiments in the $\mathfrak{a}$-series with a low degree of fragmentation produce a lot of sand in the impact, despite the relatively intact block. In contrast, intact samples in $\mathcal{F}$-series do not produce sand on impact. Possibly, this observation illustrates the effect of localized crushing of material at impact, mentioned above. That is, the samples showing a low degree of fragmentation in $\mathfrak{a}$-series are relatively thick, so that they do not break easily in tension. However, their cohesions are relatively low, which causes larger amounts of localized crushing than samples of higher cohesions. The effect of this localized crushing on the mobility appears negligible as no strong difference is observed between the travel distance and runout for the experiments from $\mathfrak{a}$ and $\mathcal{F}$-series.

Similar to the normalized area, the position of the front of the deposits (Figure 3.7b) increases due to spreading with increasing degree of fragmentation. It is interesting to note though, that the increase of the front position appears to saturate, or even decrease somewhat, as the degree of fragmentation increases above $m_c \approx 5$. This is in contrast to the area of the deposits, which steadily increases. Likely, this is caused by the fact that the experimental deposits are not continuous, but are largely made up of discrete fragments which has spread over the plate. This means that, although the front does not advance any further with increasing m_c, the area can still increase by adding more fragments and sand.

Comparing the travel distance of the samples' center of mass with their degree of fragmentation shows that the travel distance is reduced as the fragmentation is increased (Figure 3.5). Further, the collapse of the data from both $\mathfrak{a}$ and $\mathcal{F}$-series suggests that the degree of fragmentation is a controlling parameter for the final position of the center of mass. The experiments with higher basal friction generally show a shorter travel distance than the experiments on glass plates, but are seen to follow the same trend. These observations suggest that the travel

distance is simply dependent on the degree of fragmentation and the basal friction. Notice, we cannot say whether the reduction of travel distance is directly caused by the fragmentation process, or indirectly by the increase of internal friction. Likely, the reduction of travel distance is a combination of both.

3.6.2 Energy budget

The energy consumption related to the fragmentation shows an increase with the degree of fragmentation. For $m_c < 5$, a rapid increase of the fragmentation energy with the degree of fragmentation is observed. In contrast, at high degrees of fragmentation ($m_c > 5$), the fragmentation energy appears to level off. The fragmentation energy calculated for our experiments is observed to range from zero to approximately 25 % of the potential energy. This is in the same range as that estimated by *Locat et al.* (2006) (20 %) and *Crosta et al.* (2007) (1-30 %) from field observations of rock avalanches.

In Figure 3.8, two modified theoretical models have been fitted to the data. The blue line gives the best fit of a modified Kick's equation, which applies to coarse material (*Locat et al.*, 2006; *Crosta et al.*, 2007)

$$E_{Kick} = K_{Kick} log\,(m_c) \tag{3.12}$$

where K_{Kick} is constant. The best fit shown in Figure 3.8 gives $K_{Kick} = 0.08$. The red line gives the best fit of a modified Gama's equation, which is designed for blasting rocks. (*Locat et al.*, 2006)

$$E_{Gama} = K_{Gama}\sqrt{m_c} \tag{3.13}$$

where K_{Gama} is a constant called the fragmentability, and is defined as the threshold related to the energy needed to break the material along its weakest links. The best fit shown in Figure 3.8 gives $K_{Gama} = 0.06$. Of the two equations, Kick's provides the best fit, especially for the low degrees of fragmentation. The energy budget (Equation 3.9) can therefore be approximated with $W = W_\mu + W_i + W_f$, where W_μ is energy dissipated by basal friction, W_i is given by Equation 3.10 and W_f is given by Equation 3.12.

3.6.3 Mobility

The mobility of the samples is determined by how far they travel, and has previously been defined as $\mathcal{M} = L_f/H$ (*Staron and Lajeunesse*, 2009), i.e. by the runout of the front of the deposits normalized by its fall height. In our experiments, both H and l are constant, and conversion from our measure of the front ($\mathcal{L}_f$) and $\mathcal{M}$, is trivial. With this definition, the mobility of our experimental samples is observed to increase for $m_c < 5$ but to level off, or perhaps decrease somewhat, as m_c increases above 5 (Figure 3.7).

This measurement of the mobility, though relevant in understanding the reach of a deposit, does not consider the energy budget of the sample, which is characterized by the samples' center of mass. This is an important difference, because the energy lost to fragmentation is observed to increase leading to shorter travel lengths of the center of mass, however, the mobility is

seen to increase. The cause of this difference is the increased spreading of the deposits with increased degree of fragmentation. This shows an important result: even though the process of fragmentation consumes energy, which is consistent with the physics of fragmentation, the effect of fragmentation increases the mobility of gravitational rock movement.

3.6.4 Thresholds and regimes of fragmentation

The observation that m_c, which reflects the degree of fragmentation, is close to 1 for experiments with low aspect ratios or high cohesions (see Figure 3.5) suggests that a threshold for fragmentation exists, similar to what was suggested by *Wang and Tonon* (2010). That is, for samples with $\mathfrak{a} < 2$ or $\mathcal{F} < 0.03$ no fragmentation is expected to occur. Considering that we vary the aspect ratios and cohesions, rather than the impact velocity, shows that the threshold is not only a function of the available energy, but also of the geometry and strength of the material.

Interestingly, even after the threshold for fragmentation is reached, there appear to be two regimes of fragmentation: a shift of trends is observed in the relative area (Figure 3.6), relative travel distance (Figure 3.7a), relative runout (Figure 3.7b), and fragmentation energy (Figure 3.8) at $m_c \approx 5$. In the case of the area, this is reflected from the observed separation of the $\mathfrak{a}$-series and $\mathcal{F}$-series for low degrees of fragmentation, when the data points from $\mathcal{F}$-series suddenly fall to lower values. For the other three examples, the travel distance, runout and fragmentation energy are all seen to strongly depend on the degree of fragmentation for $m_c < 5$, but appears almost independent of m_c as it increases above 5. These results possibly reflect a continuous transition: the strong dependence on the degree of fragmentation for $1 < m_c < 5$ represents the transition between an intact but damaged block ($m_c \approx 1$) to a highly fragmented, granular material ($m_c \gg 1$). Possibly, these two regimes can be linked to the suggested phase transition from a damaged to fragmented state (*Kun and Herrmann*, 1999).

3.6.5 Comparison with earlier models

Many experimental models of rock slides use granular material which is released down a chute (e.g. *Davies and McSaveney*, 1999; *Manzella and Labiouse*, 2012). Compared to our experiments, granular models represent the completely fragmented case – with no remaining cohesion. In this respect, our models are simply extensions of the granular models by including the cohesion as a variable. To the authors' knowledge, this is the first time that the material strength has been considered on the transport of rock masses under gravity.

Previously, we compared the differences between three typical experiments of varying strength: no cohesion (i.e. sand), intermediate cohesion (3.5 ± 2.2 kPa) and high cohesion (360 ± 72 kPa) (*Haug et al.*, 2014). The results showed that the center of mass of a fragmenting material traveled much further than sand, but an even longer travel length was observed for the strongest material, as has been showed again here. The higher mobility of fragmenting models compared to pre-fragmented ones is similar to what was found by *Bowman et al.*

(2012). However, it is arguable whether a direct comparison between models with and without cohesion is fair due to their different dynamics. Nevertheless, these studies show the relevance of considering fragmentation in gravitational rock movements.

The models of *Bowman et al.* (2012), which address the spreading of rock avalanches with dynamic fragmentation, are similar to our models. In their models, blocks of cohesive brittle coal are released and travel down a slope before they impact and fragment on a horizontal plate. Unlike our models, their models require a centrifuge to cause fragmentation. *Bowman et al.* (2012) reported an acceleration of the material after fragmentation, and that the acceleration scaled with the degree of fragmentation. We do not see this in our models. Although the fragments in the front appear to lose little velocity through the impact, there is no sign of an increase of velocity. Possibly, this discrepancy can be caused by differences between experiments in a centrifuge and those under normal gravity, or by the different material used in the experiments. *Bowman et al.* (2012) suggested that the increased velocity of the front due to fragmentation could be caused by material pushing from behind. This effect could possibly be larger in a centrifuge than under normal gravity. Alternatively, one could speculate whether the increased gravity in the centrifuge can elastically compress the coal blocks used in their experiments, and that this elastic strain energy can be converted into kinetic energy upon fragmentation. If this is the case, our models, which act under normal gravity, cannot be expected to recreate their results.

3.6.6 Comparison with nature

Our models are simple, and are not meant to model the full complexity of gravitational rock movement. The models aim to study the process of fragmentation occurring self-consistently, in a simple sliding setting. It is worth noting though, that the process of fragmentation may occur on all scales and in all types of gravitational rock movement. Therefore, despite the lack of a direct comparison between our models and natural systems, the process of fragmentation studied in our models can be relevant for a multitude of natural systems. The fact that our results show that the mobility is determined simply by the degree of fragmentation and the friction suggests that despite the difference in fragmentation mechanisms the models of fragmenting gravitational rock movements may be generally applicable to situations where fragmentation occurs. Even so, there are certainly systems to which our models apply more readily, and in the following we consider those.

In general, our experiments model the incremental motion of an intact piece of rock traveling over topography, i.e. slope break, causing it to break apart. They can therefore be considered the detailed study of *one* event of fragmentation that may, or may not, be followed by similar events.

In our experiments fragmentation occurs by impact; however, they are different from free-falling objects hitting the ground, such as the models by *Wang and Tonon* (2010). In our models, the impact with the horizontal surface is not orthogonal, but guided by an inclined plane. Nevertheless, the deformation in our models is driven by the oblique impact and travel through a change in slope, suggesting that they may also be applicable to rock falls.

The observation that fragmentation of thin samples occurs more readily than thicker ones (Figure 3.5a) suggests that elastic bending is a dominating mechanism for fragmentation in our models. This mechanism is usually not recognized as relevant for systems such as rock slides and rock avalanches. The exception might be in the initial stages of the movement, i.e. immediately after failure. At this point, the material can still be more or less intact and will move out of the failure zone, which can be considered as a block moving over topography. Our models can therefore provide insights into the primary fragmentation and the further mobility of rock slides. In that case, our models suggest that the energy consumed in the initial fragmentation may not be negligible, since as much as 25 % of the potential energy can be consumed by it. Notice, not all rock slides fail as an intact piece, some rock slides appear to simply collapse, e.g. Randa rock slide (*Eberhardt et al.*, 2004). Our models would not apply to these situations.

Another system to which our models may apply more directly are the rock planar (translational) slides (*Hungr et al.*, 2013). These rock slides are structurally controlled, sliding on a planar rupture surface. The rock planar slides experience limited internal deformation during initial failure, and the material leaves the failure site as an intact block of rock. During transport, however, the block can break apart due to the travel over topography and impacts. For these systems, our models may help to explain whether a block will remain intact throughout its travel, or whether it will fragment, and potentially turn into a granular flow. Though such an analysis is outside the scope of this paper, understanding this transition is important for the understanding and modeling of block slides, and deserves further investigation in the future.

3.7 Conclusions

We have performed lab-scale fragmentation experiments of gravitational rock movements, using a new rock analogue material. From dimensional analysis, we derived a set of dimensionless parameters that characterize the models, three of which ($\mathfrak{a}$, $\mathcal{F}$ and μ) are varied here to see their effect on the mobility of gravitational rock movements.

Our results showed that the degree of fragmentation is a function of both the material strength and geometry of the movement, and that fragmentation occurs only above a threshold of this value. The relative area and the relative front position of the deposits are observed to increase with the degree of fragmentation. In contrast, the travel distance of the center of mass is observed to decrease, as more fragmentation occurs.

The latter observation is caused by the increase of energy consumption with the degree of fragmentation. The fragmentation energy is found to follow a logarithmic curve (Equation 3.12), which increases rapidly as $1 < m_c < 5$, but levels off at around 25 % of the potential energy for system with $m_c > 5$.

Importantly, despite the lost energy to fragmentation, the runout of the front increases with the degree of fragmentation. This causes an increased mobility due to fragmentation.

3.8 Appendix: Limitations and uncertainties

Even though providing an exact number of the uncertainty of our method is difficult, estimates of the uncertainty can be taken from the spread of data from a mean trend line in the figures (Figure 3.5, 3.6, 3.7 and 3.8). There may be several causes of uncertainty, and here we point out the ones that are expected to be most significant. However, it should be pointed out that the spread of data is not purely a result of measurement errors. Experiments will always have a natural variability of results due to small differences in initial conditions. Because of this natural variability, as well as measurement errors, many experiments are needed to produce reliable results.

In our analysis, the position of the center of mass is calculated from Equation 3.8, where the mass and position of individual fragments are found through image analysis. Calculation of the mass of fragments requires conversion from the 2-dimensional images to volume using the equivalent diameter (Equation 3.7) and an assumption that small fragments are spherical. Errors may arise from this, and the center of mass positions reported in the Results section above are not exact. Additional error may also arise from the image analysis, by for example failing to recognize some fragments.

When calculating the fragmentation energy (Figure 3.8) we assumed that the work related to the impact, W_i, was constant for all experiments (Equation 3.11). The justification of this assumption was that a difference in energy consumption between an intact and a fragmenting sample is due to the fragmentation process, and should therefore be considered part of the fragmentation energy. Nevertheless, the value of W_i cannot currently be measured in our experiments. To rectify this, experiments are in progress where the samples' movement is recorded by means of seismic sensors.

In the models reported here, it has been assumed that the rock mass in gravitational rock movements can be modeled as uniform rock, with an effective strength characterized by bulk cohesion. This is not realistic for many natural gravitational rock movement since most rocks contain joints (*Eberhardt et al.*, 2004). A more realistic setup might be a collection of brittle blocks traveling down the chute, similar to the model of *Bowman et al.* (2012) and *Imre et al.* (2010). However, as this would increase the complexity of our models, we have kept it as simple as possible: by only considering one block. In the future, tests should be done where a collection of fragmentable particles is used.

Compared to natural systems, neither the geometry of the sample nor the chute are realistic. However, this is a common setup for the study of rock slides in experimental models (e.g. *Davies and McSaveney* (1999); *Manzella and Labiouse* (2012); *Imre et al.* (2010); *Bowman et al.* (2012)), which allow us to compare our results to previous models in the literature.

Acknowledgments

The authors would like to thank to Frank Neumann and Thomas Ziegenhagen for construction and technical assistance. The work is supported by the Helmholtz Graduate Research School

GEOSIM and the German Ministry for Education and Research (BMBF, FKZ03G0809A).
The data for this paper are available by contacting the corresponding author.

References

Agliardi, F., and G. Crosta (2003), High resolution three-dimensional numerical modelling of rockfalls, *Int. J. Rock Mech. Min.*, *40*(4), 455–471, doi:10.1016/S1365-1609(03)00021-2.

Åström, J. A. (2006), Statistical models of brittle fragmentation, *Adv. Phys.*, *55*(3-4), 247–278, doi:10.1080/00018730600731907.

Barenblatt, G. I. (2003), *Scaling*, vol. 34, Cambridge University Press.

Bowman, E. T., W. A. Take, K. L. Rait, and C. Hann (2012), Physical models of rock avalanche spreading behaviour with dynamic fragmentation, *Can. Geotech. J.*, *49*(4), 460–476, doi:10.1139/t2012-007.

Crosta, G. B., P. Frattini, and N. Fusi (2007), Fragmentation in the Val Pola rock avalanche, Italian Alps, *J. Geophys. Res.*, *112*, F01,006, doi:10.1029/2005JF000455.

Dammeier, F., J. R. Moore, F. Haslinger, and S. Loew (2011), Characterization of alpine rockslides using statistical analysis of seismic signals, *J. Geophys. Res.*, *116*(F4), F04,024, doi:10.1029/2011JF002037.

Davies, T. R., and M. J. McSaveney (1999), Runout of dry granular avalanches, *Can. Geotech. J.*, *36*(2), 313–320, doi:10.1139/t98-108.

Davies, T. R., and M. J. McSaveney (2009), The role of rock fragmentation in the motion of large landslides, *Eng. Geol.*, *109*(1-2), 67–79, doi:10.1016/j.enggeo.2008.11.004.

Deparis, J., D. Jongmans, F. Cotton, L. Baillet, F. Thouvenot, and D. Hantz (2008), Analysis of Rock-Fall and Rock-Fall Avalanche Seismograms in the French Alps, *B. Seismol. Soc. Am.*, *98*(4), 1781–1796, doi:10.1785/0120070082.

Eberhardt, E., D. Stead, and J. Coggan (2004), Numerical analysis of initiation and progressive failure in natural rock slopes – the 1991 Randa rockslide, *Int. J. Rock. Mech. Min.*, *41*(1), 69–87, doi:10.1016/S1365-1609(03)00076-5.

Haug, Ø. T., M. Rosenau, K. Leever, and O. Oncken (2014), Modelling Fragmentation in Rock Avalanches, *Landslide Science for a Safer Geo-Environment*, *2*, 93 – 100, doi:10.1007/978-3-319-05050-8_16.

Hungr, O., S. Leroueil, and L. Picarelli (2013), The Varnes classification of landslide types, an update, *Landslides*, *11*(2), 167–194, doi:10.1007/s10346-013-0436-y.

Imre, B., J. Laue, and S. M. Springman (2010), Fractal fragmentation of rocks within sturzstroms: insight derived from physical experiments within the ETH geotechnical drum centrifuge, *Granul. Matter*, *12*(3), 267–285, doi:10.1007/s10035-009-0163-1.

Kilburn, C. R. J. (2001), *The flow of giant rock landslides*, 245–265 pp., Elsevier B.V.

Kun, F., and H. Herrmann (1999), Transition from damage to fragmentation in collision of solids, *Phys. Rev. E*, *59*(3), 2623–2632, doi:10.1103/PhysRevE.59.2623.

Locat, P., R. Couture, S. Leroueil, J. Locat, and M. Jaboyedoff (2006), Fragmentation energy in rock avalanches, *Can. Geotech. J.*, *43*(8), 830–851, doi:10.1139/t06-045.

Lucas, A., A. Mangeney, and J. P. Ampuero (2014), Frictional velocity-weakening in landslides on Earth and on other planetary bodies., *Nat. Com.*, *5*, 3417, doi:10.1038/ncomms4417.

Manzella, I., and V. Labiouse (2012), Empirical and analytical analyses of laboratory granular flows to investigate rock avalanche propagation, *Landslides*, (January), doi:10.1007/s10346-011-0313-5.

Nocilla, N., A. Evangelista, and A. Scotto di Santolo (2009), Fragmentation during Rock Falls: Two Italian Case Studies of Hard and Soft Rocks, *Rock Mech. Rock Eng.*, *42*(5), 815–833, doi:10.1007/s00603-008-0006-0.

Pollet, N., and J.-L. Schneider (2004), Dynamic disintegration processes accompanying transport of the Holocene Flims sturzstrom (Swiss Alps), *Earth Planet Sc. Lett.*, *221*(1-4), 433–448, doi:10.1016/S0012-821X(04)00071-8.

Schellart, W. (2000), Shear test results for cohesion and friction coefficients for different granular materials: scaling implications for their usage in analogue modelling, *Tectonophysics*, *324*(1-2), 1–16, doi:10.1016/S0040-1951(00)00111-6.

Staron, L., and E. Lajeunesse (2009), Understanding how volume affects the mobility of dry debris flows, *Geophys. Res. Lett.*, *36*(12), 2–5, doi:10.1029/2009GL038229.

Timár, G., F. Kun, H. a. Carmona, and H. J. Herrmann (2012), Scaling laws for impact fragmentation of spherical solids, *Phys. Rev. E*, *86*(1), 016, 113, doi:10.1103/PhysRevE.86.016113.

Varnes, D. (1978), Slope movement types and processes, *Trans. Res. B.*

Wang, Y., and F. Tonon (2010), Discrete Element Modeling of Rock Fragmentation upon Impact in Rock Fall Analysis, *Rock Mech. Rock Eng.*, *44*(1), 23–35, doi:10.1007/s00603-010-0110-9.

Chapter 4

On the transition from solid to granular: a one-parameter description of the rockslide to flow evolution

Abstract

Fragmentation of rockslides may cause significant changes to their bulk material properties, energy budget and travel length. Previous studies of fragmentation of rockslides commonly use the final products to estimate the energy consumed by the fragmentation process. However, little is known of the time-evolution of this process, which transforms the initially quasi-intact rock into multiple fragments. In particular, how do the initial conditions affect the fragmentation process? Here, we present an integrated study of experimental and analytical models of fragmentation of rockslides. The experiments show that the degree of fragmentation depends on geometry, kinetic energy and material strength of the experimental slides. The analytically derived parameter presented in this paper collapses the experimental results into a single function. From the new analytical expression, the degree of fragmentation and the energy consumed by the fragmentation, can be predicted from initial conditions.

Keywords
Rockslides, Rockfalls, Fragmentation, Analytical model

Ø. T. Haug, M. Rosenau, K. Leever, O Oncken

Intended for submission to *Geophysical Research Letters*

4.1 Introduction

The process of fragmentation can occur in all types of gravitational rock movements, on scales ranging from pebbles to mountains. Fragmentation of rocks during rockslides is known to lead to changes in their bulk material properties, travel length (*Pollet and Schneider*, 2004) and energy budget (*Haug et al.*, under review JGR). Thus, fragmentation is highly relevant for the transport of rocks under gravity.

When a rock mass fragments during transport, changes in the bulk material properties due to fragmentation induce changes in the mode of transport. Most evident is the loss of cohesion caused by the breaking apart of the rock, which allows the material to spread and undergo internal deformation. Illustrating the relevance of this transition are the rock avalanches, e.g. the Seymareh rock avalanche in Iran (*Roberts and Evans*, 2013; *Hungr et al.*, 2013), where several stacked blocks of rocks fragmented during failure and transport, causing the planar slide to transform into a rock avalanche. In order to model such transport events, being able to predict the degree of fragmentation of the rock mass would be largely beneficial. However, little is known of the conditions under which the fragmentation occurs.

Fragmentation consumes energy, called the fragmentation energy. For its estimation, *Locat et al.* (2006) and *Crosta et al.* (2007) used the size distribution of the fragments in the deposits and various empirical and theoretical expressions. Although this approach is helpful to gain insights into energy budgets of natural events, it can only estimate the fragmentation energy after the fragmentation has occurred. To be able to predict the fragmentation energy of rockslides, one would first need to predict the degree of fragmentation.

Here, we present an integrated study of analogue and analytical models of fragmenting rockslides. The analogue models reveal the existence of three different kinematic regimes related to the degree of fragmentation. The degree of fragmentation is found to depend on several variables, such as geometry of the slide and its material strength. To unify the contributions of these variables, we derive a new parameter by considering the peak tensile stress in an elastic block, normalized by its cohesion. The new parameter, in combination with the experimental results, allows us to derive a scaling law for the degree of fragmentation. This scaling law can be used to predict the degree of fragmentation and the fragmentation energy from initial conditions.

4.2 Background: Experiments with three kinematic regimes

Here, only a brief description of the experimental setup is given, a more detailed description has been reported in a previous publication (*Haug et al.*, under review JGR). In the experiments, rockslides are modeled by the release of a block of a brittle rock analogue material (*Haug et al.*, 2014) down a 1 meter long slope at an angle of 45°. After accelerating down the slope, the block impacts on a horizontal plate, on which the sample fragments, spreads and comes to rest.

Images of three experiments with different degrees of fragmentation, and representing three

$\mathfrak{a}$	Aspect ratio of sample ($= l_0/h$)
D	Flexural rigidity.
F	Shear stiffness.
$\mathcal{F}$	Ratio between specific potential energy and cohesion (See Equation 4.1).
g	Gravitational acceleration.
h	Thickness of slide.
H	Fall height of the slide.
$\mathcal{H}$	Relative fall height ($= H/l_0$).
l	Length of the slide, in the direction of travel.
K	Constant in fragmentation energy equation.
M	Bending moment of plate.
m_c	Characteristic fragment size, ratio between mass of largest fragment and total mass. Reflects the degree of fragmentation.
r	Radius of the turn of the sample through the corner.
S_{eff}	Fragility parameter.
u_i	Displacement of plate in direction i.
w	Deflection of plate.
x	Position in plate.
α	Angle of the slide with respect to horizontal.
θ	Angle of the slope.
κ	Constant in fragmentation energy equation $= (2/5)K$.
μ	Coefficient of basal friction.
ν	Poisson ratio.
$\xi(\theta)$	Proportionality function between r and l.
ρ	Density.
σ_{max}	Approximate peak tensile stress.
ϕ	Potential function.

Table 4.1: Notation

different kinematic regimes, are presented in Figure 4.1. In the upper row of Figure 4.1(a-d), the released material is cohesionless sand (effective cohesion in the order of a few tens of Pa). The sample is observed to collapse immediately at the point of release, and the following transport can be described as granular flow: expanding and extending on the slope and horizontal plane, respectively. This regime is referred to as *immediate collapse*. A different kinematic regime is observed for cohesive but weak sample (Figure 4.1e-h), which remains intact during acceleration down the slope, but fragments upon impact on the horizontal plane. This regime is referred to as *dynamic fragmentation*. The last kinematic regime observed in the experiments is referred to as *elastic block*, and is related to samples which are sufficiently strong as to experience only limited damage (Figure 4.1i-k).

Different regimes are found to be related to the degree of fragmentation. Therefore, to predict the former, one would need to predict the latter. Existing analytical models predicting the degree of fragmentation (e.g. *Grady*, 1982) often require information about the system, which is not readily available, e.g. the strain rate. An alternative (or supplement) to analytical models are the empirical scaling laws. *Locat et al.* (2006) suggested that the degree of fragmentation of rock avalanches scales well with a parameter equivalent to

$$\mathcal{F} = \frac{\rho g H}{C} \tag{4.1}$$

where ρ is the density, g is the gravitational acceleration, H is the fall height and C is the cohesion. Recently, we performed experiments of fragmentation of a sliding block of brittle material (*Haug et al.*, under review JGR), confirming the relevance of this parameter (Figure 3.5a). However, the parameter $\mathcal{F}$ was seen to neglect the effects of the geometry of the sample: Figure 3.5b shows that the same range of degree of fragmentation can be achieved by varying the aspect ratio ($\mathfrak{a}$) of the sample as by varying $\mathcal{F}$. Consequently, this parameter is not sufficient for scaling initial conditions to the degree of fragmentation. Rather, a combination of both $\mathcal{F}$ and $\mathfrak{a}$ is needed.

4.3 An analytical model for fragmentation

Our goal is to understand how $\mathfrak{a}$ and $\mathcal{F}$ act together in the fragmentation process. To do this, we derive an analytical model of fragmenting rockslides, which considers the motion of an elastic plate over a sudden change of slope angle (θ) measured from the horizontal (see Figure 4.3a), similar to the setup of the experiments. In the model, the samples' travel past the corner is modeled as rotation of an elastic plate. To determine the susceptibility to fragmentation, we evaluate the peak tensile stress within the elastic plate with respect to its material strength.

The tensile stress is calculated from the 1-dimensional Kirchhoff's theory (see e.g. *Ventsel and Krauthammer* (2001); *Vasil'ev* (1998)). This theory assumes that the thickness of the plate, h, is much smaller than the length of the plate l_0, i.e. $h \ll l_0$. This assumption is not always met by our samples, or by material in rockslides in general. However, our aim is

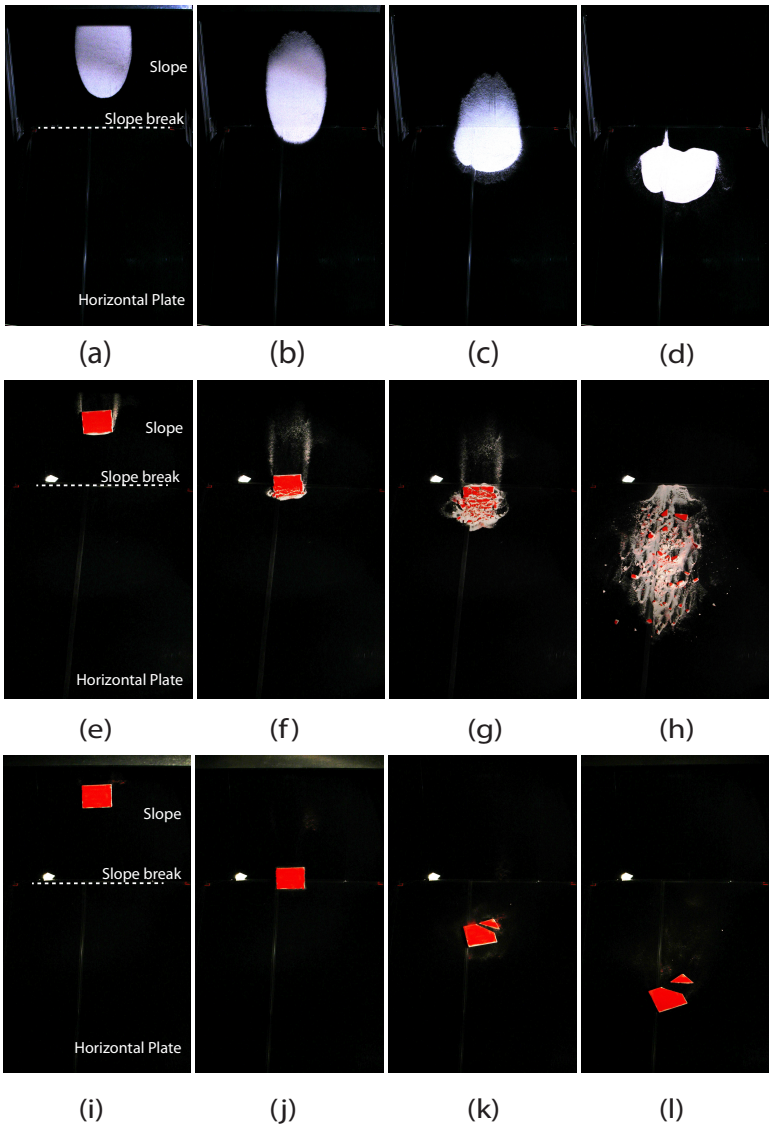

Figure 4.1: Three kinematic regimes. (a-d) *Immediate collapse*: The sample undergoes complete failure at the point of release, leading to a granular flow throughout its transport. (e-h) *Dynamic fragmentation*: The sample stays intact while accelerating down the slope, but upon impact on the horizontal plane it fragments, transforming the material from an elastic block into a granular flow. (i-k) *Elastic block*: The sample remains intact during its entire travel path, deforming elastically upon impact on the horizontal plane.

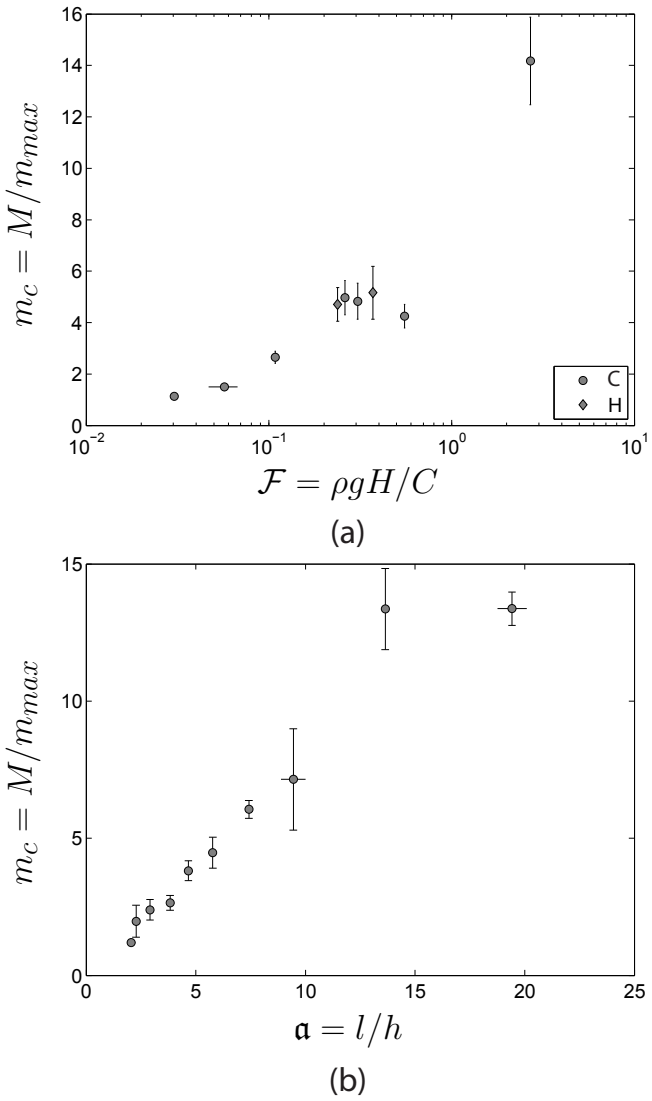

Figure 4.2: The characteristic fragment size, m_c, which reflects the degree of fragmentation, plotted against (a) the potential energy normalized by cohesion, $\mathcal{F}$, and (b) aspect ratio, $\mathfrak{a}$. The characteristic fragments size $m_c = m_{max}/M$ is the ratio between the mass of the largest fragment divided by the mass of the total sample, and reflects the degree of fragmentation. In (a), circles indicate experiments where the cohesion is varied, and diamonds where fall height is varied. For a comprehensive description of the experiments, we refer to *Haug et al.* (under review JGR).

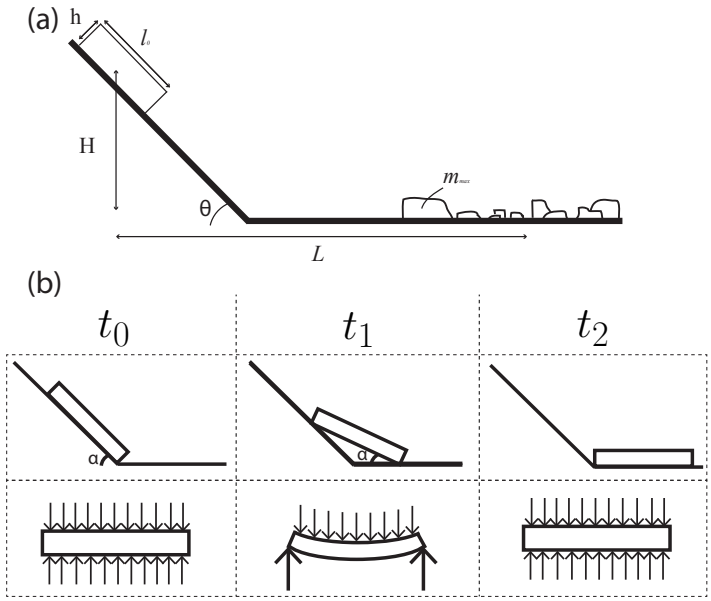

Figure 4.3: Sketch of the model. In (a), the plate at its initial position and the deposits after it has come to rest are shown. In (b), 3 time steps of the plate rotating (upper row) and elastically bending (lower row) while traveling through the corner are shown.

not to get an exact description of the stresses in the samples, but to determine the degree of fragmentation. We will argue below that it is sufficient to consider the stress derived from this simple theory, modified by a factor that accounts for the thickness of the plate.

4.3.1 Tensile stress from the 1-dimensional Kirchhoff's model

The 1-dimensional Kirchhoff equation gives that

$$D\frac{d^4w}{dx^4} = \frac{d^2M}{dx^2} = -q \tag{4.2}$$

where D is the flexural rigidity of the plate, w is the deflection of the plate with respect to the horizontal, M is the bending moment, q is the load on the plate and x the parametrized coordinate along the sample. Integrating Equation 4.2 twice, and using the boundary conditions that there is no stresses at the edges, i.e. $M(x = 0) = M(x = l_0) = 0$, gives the bending moment:

$$M = \frac{1}{2}q\left(l_0x - x^2\right) \tag{4.3}$$

The load, q, on the plate is caused by the gravity on the plate as well as the additional

acceleration caused by rotating the sample through the corner.

$$q = \frac{\rho h}{\cos\alpha}\left(g + \frac{v_{imp}^2}{r}\right) \tag{4.4}$$

where α is the angle of the sample with respect to the horizontal (see Figure 4.3b), ρ is the density, g is the gravitational acceleration, v_{imp} is the velocity of the sample as it enters the corner and r is the radius of the turn of the sample through the corner. Notice, in Equation 4.4 it is assumed that the rotation is circular, so that the additional rotational acceleration can be expressed as v_{imp}^2/r. The radius can be approximated by considering the position of the center point of the plate in 3 time steps during rotation. This leads to

$$r = l_0\xi(\theta) \tag{4.5}$$

where

$$\xi(\theta) = \sqrt{\frac{1}{4} - \Phi(\theta) + \left[1 + \tan^2\left(\frac{\theta}{2}\right)\right]\Phi(\theta)} \tag{4.6}$$

and

$$\Phi(\theta) = \frac{2\cot^2(\theta)}{2\left[1 + 4\cot^2(\theta)\right] - \tan^2(-\theta/2)\sqrt{1 + 4\cot^2(\theta)}} \tag{4.7}$$

The tensile stress can be shown to be at a minimum at the base of the sample, and is given as

$$\sigma_{xx}^{max} = -\frac{6}{h^2}M \tag{4.8}$$

In the following, we are only interested in the magnitude of the tensile stress, and for convenience, the negative sign is neglected. Inserting Equation 4.3 into Equation 4.8, and using that the point of peak tensile stress along the sample is at $x = l_0/2$, gives

$$\sigma_{max} = \frac{3}{4}\frac{l_0^2}{h^2 cos\alpha}\left(\rho g h + \frac{\rho v_{imp}^2 h}{\xi(\theta) l_0}\right) \tag{4.9}$$

where the expression of q from Equation 4.4 and 4.5 has been used.

4.3.2 Accounting for the thickness of the samples

A more complicated theory, which does not require very thin plates is the 3-dimensional Reissner's theory (*Reissner*, 1944, 1945). In this theory, the displacement in x, y and z direction are given by $u_x = zv_x$, $u_y = zv_y$ and $u_z = w(x, y)$, respectively. The v_x and v_y are the angles between a line orthogonal to the mid-surface (on which $\sigma_{xx} = 0$) and the respective normal vectors (*Vasil'ev*, 1998). The differential equation in this case is

$$D\Delta\Delta\phi = q \tag{4.10}$$

where $\Delta = \frac{\partial^2}{\partial x^2} + \frac{\partial^2}{\partial y^2}$ is the Laplace operator and ϕ is the potential function given by

$$v_x = \frac{\partial \phi}{\partial x}; \quad v_y = \frac{\partial \phi}{\partial y} \tag{4.11}$$

It can be shown that the potential function relates to the deflection w as

$$w = \phi - \frac{D}{F}\Delta\phi \tag{4.12}$$

where D is the *flexural rigidity* and F describes the *shear stiffness* of the plate (*Vasil'ev*, 1998; *Ventsel and Krauthammer*, 2001). Through an asymptotic analysis *Vasil'ev* (1998) showed that

$$w = \phi - \left(\frac{h}{l_0}\right)^2 (6 - 6\nu)^{-1} \Delta\phi \tag{4.13}$$

where ν is the Poisson ratio. Equation 4.13 demonstrates how the factor $(h/l_0)^2$ causes the second term on the right-hand side of Equation 4.13 to become non-negligible for thicker plates. To account for this factor, we multiply the tensile stress derived using Kirchhoff's model in Equation 4.14 with $(l_0/h)^2$:

$$\frac{l_0^2}{h^2}\sigma_{max} = \frac{3}{4}\frac{l_0^4}{h^4 cos\alpha}\left(\rho g h + \frac{\rho v_{imp}^2 h}{\xi(\theta) l_0}\right) \tag{4.14}$$

Notice, Equation 4.14 gives the peak tensile stress for a perfect elastic thin plate multiplied with the dimensionless factor l_0^2/h^2. As a result, Equation 4.14 no longer reflects the tensile stress. Even so, it still retains a relative measure of the tensile stress, which is sufficient for our analysis.

4.3.3 A failure criterion

We assume that failure occurs when $S_{eff} = (l_0^2/h^2)(\sigma_{max}/C) > k$, where C is the cohesion of the material and k is a constant. The angle at failure $\alpha = \alpha_f$ is difficult to determine, but will, in general, be limited between θ and $0°$. In the following, we simply put $\alpha = \theta$. Thus, at failure, from Equation 4.14 we have

$$S_{eff} = \frac{3}{4}\frac{l_0^4}{h^4 cos(\theta)}\left(\frac{\rho g h}{C} + \frac{\rho v_{imp}^2}{C}\frac{h}{\xi(\theta) l_0}\right) \tag{4.15}$$

Equation 4.15 can be rewritten using the dimensionless parameters $\mathfrak{a}$ and $\mathcal{F}$ as

$$S_{eff} = \frac{3}{4}\frac{\mathfrak{a}^3 \mathcal{F}}{\cos(\theta)}\left[\mathcal{H}^{-1} + 2\xi(\theta)^{-1}\left(1 - \frac{\mu}{\sin(\theta)}\right)\right] \tag{4.16}$$

where we have used that $v_{imp}^2 = 2gH(1 - \mu/\sin(\theta))$, where mu is the basal coefficient of friction, and the scaled fall height $\mathcal{H} = H/l_0$.

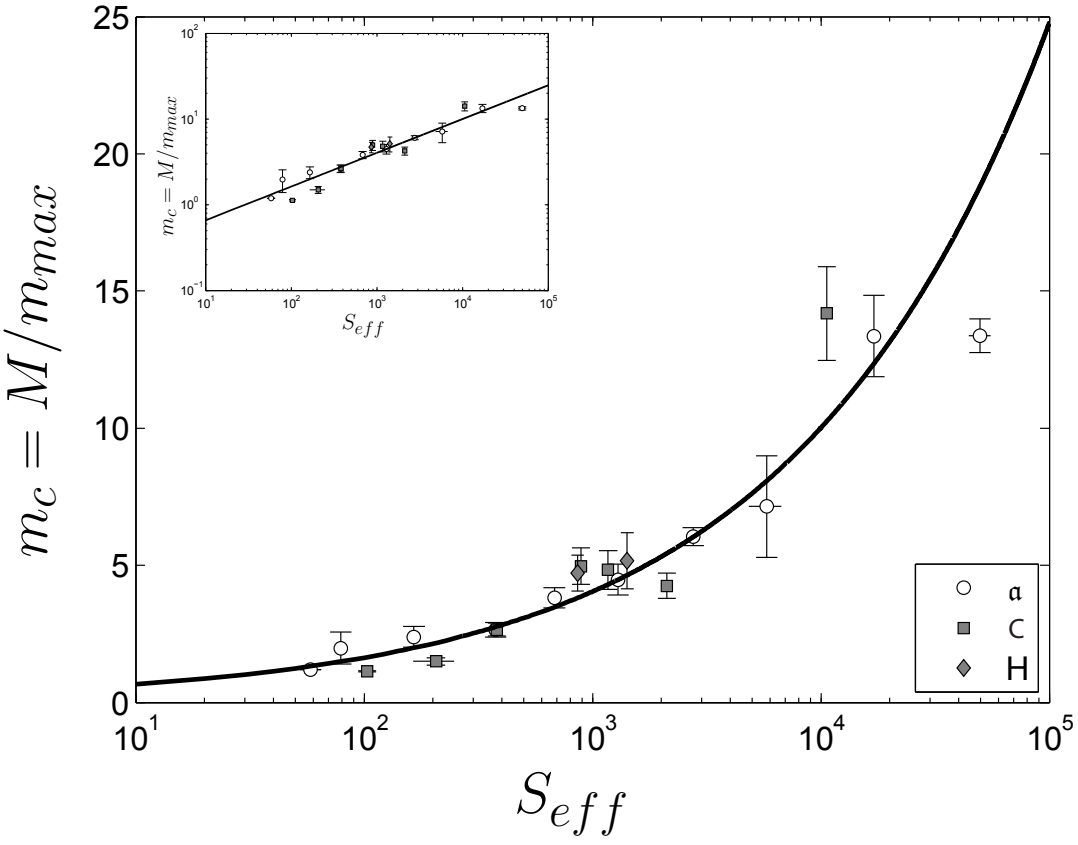

Figure 4.4: Characteristic fragment size m_c plotted against S_{eff}. Circles indicate experimental the results when the thickness to length ratio is varied, squares when the tensile strength is varied, and diamonds when the impact velocity is varied. Insert: same plot, but with logarithmic y-axis

4.3.4 Comparing the analytical models with the analogue model

The characteristic fragment size (m_c) for the experiments presented in Figure 4.2, are plotted in Figure 4.4 against their respective values of S_{eff}. The two series of experiments are seen to collapse onto one curve. This suggests that our analytically derived parameter S_{eff} is able to capture the governing mechanism of the fragmentation process, and that it can be used for predicting the fragment sizes.

Based on the data distribution in Figure 4.4, we suggest that $m_c = c_1 S_{eff}^{c_2}$. Using a linear regression of the logarithms of m_c and S_{eff} gives the two constants $c_1 = 0.27 \approx 1/4$ and $c_2 = 0.39 \approx 2/5$, so that

$$m_c = \frac{1}{4} S_{eff}^{2/5} \tag{4.17}$$

4.3.5 Predicting fragmentation energy from initial conditions

Previously, *Haug et al.* (under review JGR) showed that the fraction of potential energy consumed by fragmentation could be expressed as

$$W_f = Klog(m_c) \tag{4.18}$$

where K is a constant equal to 0.08. Since $m_c = m_{max}/M$ is used to express the fragmentation energy, it can only be measured from the final deposits. Hence, it is impossible to determine the fragmentation energy until after the fragmentation has occurred. Inserting Equation 4.17 into Equation 4.18 the fragmentation energy can be expressed by

$$W_f = \kappa log\left(\frac{S_{eff}}{4}\right) \tag{4.19}$$

where $\kappa = (2/5)K$. With this expression, the fragmentation energy can be determined solely from initial conditions.

4.4 Discussion

Here, we present a new parameter which combines the effect of the potential energy, material strength and geometry on the degree of fragmentation, by considering the tensile stresses of elastic blocks normalized by the material strength. This allows us to derive a scaling law relating the degree of fragmentation to initial conditions (Equation 4.17). From this relationship, we can apply an empirical or theoretical equation (e.g. Equation 4.18) relating the degree of fragmentation to the fragmentation energy, and can calculate the fragmentation energy (Equation 4.19), solely from initial conditions.

Based on the value of parameter S_{eff}, the kinematic regime of a rockslide can be predicted. It is observed that low values of S_{eff} yield samples which remain largely intact. Rockslides with $S_{eff} < 10^3$ are therefore expected to appear in the *elastic block* regime. In contrast, if the material easily fragments during its travel ($S_{eff} > 10^3$), the system would likely transform from a slide into a flow, and such systems are expected to appear in the *dynamic fragmentation* regime. As the cohesion of the material approaches zero, the value of S_{eff} diverges. In such cases, the material is so weak that any acceleration causes complete failure, and are therefore expected to be within the *immediate collapse* regime.

While we here have focused mainly on rockslides, the value of S_{eff} may also be relevant to determine the kinematic regime, i.e. the degree of fragmentation, for other gravitational rock movements. For example, if we consider a rockfall with a fall height of 10 m, cohesion of 10^6 Pa, aspect ratio of 1, and assuming all other parameters constant, we get a value of $S_{eff} = 2.25$, which is well within the elastic block regime. In comparison, a rockfall with a fall height of 100 m, cohesion of 10^6 Pa and an aspect ratio of 5 has a value of $2 \cdot 10^3$, i.e. within the dynamic fragmentation regime.

Our models consider only one event of fragmentation caused by tensile bending of the block. In nature, several events of fragmentation are expected to occur. However, after the

initial fragmentation of the block into a granular material, comminution and grinding likely takes over as the dominant mechanism for fragmentation. This will overprint the signal from the initial fragmentation in the final deposits, making comparison of the parameter S_{eff} to natural systems difficult. Nevertheless, an attempt to calculate the value of S_{eff} from the data from Seymareh rock avalanche presented in *Roberts and Evans* (2013) is given here. This rock avalanche consisted of several layered blocks, and its motion was described as "resembling sliding of an inclined deck of cards". Due to its more simple conditions and its similarity to our models, we only calculate S_{eff} for the overriding stronger limestone block, and will not consider the weaker rock below. To calculate the S_{eff}, we simply use initial length and thickness of the entire block, and assume a rock strength of 10^8 Pa. This gives the calculated value of S_{eff} of $2 \cdot 10^4$, which places this event within the dynamic fragmentation regime. Additionally, we calculate values of S_{eff} from the data of rock avalanches presented in *Locat et al.* (2006). In these cases, S_{eff} is found to range from $2 \cdot 10^2$ to $3 \cdot 10^4$, which suggests both the elastic block and the dynamic fragmentation regime are present in this data set. This may suggest that some of these rock avalanches only experience limited initial breakup, and that most of the fragmentation took place on a later stage during transport.

4.5 Conclusions

Analogue models of fragmenting rockslides show how such systems can be characterized in three kinematic regimes: immediate collapse, dynamic fragmentation and elastic blocks. We present a parameter, S_{eff}, that takes into consideration material strength, available potential energy and geometry of the system on the degree of fragmentation in rockslides, which allows predicting its kinematic regime from initial conditions. Additionally, we use this parameter to derive a scaling law for the fragmentation energy (Equation 4.19) such that this also can be predicted from initial conditions.

References

Crosta, G. B., P. Frattini, and N. Fusi (2007), Fragmentation in the Val Pola rock avalanche, Italian Alps, *Journal of Geophysical Research*, *112*, F01,006, doi:10.1029/2005JF000455.

Grady, D. (1982), Local inertial effects in dynamic fragmentation, *Journal of Applied Physics*, *87185*(September 1981), 322–325.

Haug, Ø. T., M. Rosenau, K. Leever, and O. Oncken (2014), Modelling Fragmentation in Rock Avalanches, *Landslide Science for a Safer Geo-Environment*, *2*, doi:10.1007/978-3-319-05050-8_16.

Haug, Ø. T., M. Rosenau, K. Leever, and O. Oncken (under review JGR), Effect of fragmentation on the mobility of gravitational mass movements: insights from analogue experiments, *Journal of Geophysical Research*.

Hungr, O., S. Leroueil, and L. Picarelli (2013), The Varnes classification of landslide types, an update, *Landslides*, *11*(2), 167–194, doi:10.1007/s10346-013-0436-y.

Locat, P., R. Couture, S. Leroueil, J. Locat, and M. Jaboyedoff (2006), Fragmentation energy in rock avalanches, *Canadian Geotechnical Journal*, *43*(8), 830–851, doi:10.1139/t06-045.

Pollet, N., and J.-L. Schneider (2004), Dynamic disintegration processes accompanying transport of the Holocene Flims sturzstrom (Swiss Alps), *Earth and Planetary Science Letters*, *221*(1-4), 433–448, doi:10.1016/S0012-821X(04)00071-8.

Reissner, E. (1944), On the theory of bending of elastic plates, *Journal of Mathematical Physics*, *23*(4), 184–191.

Reissner, E. (1945), The effect of transverse shear deformation on the bending of elastic plates, *Journal of Applied Mechanics*, *12*, 69–77.

Roberts, N. J., and S. G. Evans (2013), The gigantic Seymareh (Saidmarreh) rock avalanche, Zagros fold–thrust belt, Iran, *Journal of the Geological Society*, *170*(4), 685–700.

Vasil'ev, V. V. (1998), Classical Theory of Plates: Historical Perspective and State-Of-The-Art, *Mechanics of Solids*, *33*(3), 35–45.

Ventsel, E., and T. Krauthammer (2001), *Thin Plates and Shells*, CRC Press, doi: 10.1201/9780203908723.

Chapter 5

Variations in runout length of rock avalanches controlled by fragmentation, not basal friction

Rock avalanches are extraordinary, very large rockslides that consist of highly fragmented materials and display exceptionally long runout lengths that are found to correlate with their volume (Hsü, 1975; Hungr et al., 2013). Such volume-dependent long runouts are conventionally attributed to dynamic lowering of the effective basal friction (e.g. Kent, 1966; Shreve, 1968; Hsü, 1975; Melosh, 1979; Campbell, 1989). However, even for similar volumes, the runouts are seen to span several order of magnitude (Staron and Lajeunesse, 2009). We present a different perspective on long runout which explains existing data better: relating the runout to fragmentation and spreading of material. We show that for a given low basal friction, the runout of rock avalanches is determined by their degrees of fragmentation, even if their volume vary over two orders of magnitude. The fragmentation is observed to cause spreading, but also leads to stronger internal interactions between fragments. Consequently, the runout's dependence on fragmentation is determined by the competition between spreading and internal friction, which we incorporate into a scaling law describing runout as a function of degree of fragmentation. Due to this dependence, a strong rock that fragments travels further on the same topography than a weak rock that collapses. This shows that fragmentation plays an important role in the mobility of rock avalanches, and should be considered in their hazard assessments.

With volumes larger than 10^6 m^3, and speeds reported at over 150 km/h (Campbell, 1989),

Ø. T. Haug, M. Rosenau, K. Leever, O. Oncken

Intended for submission to *Nature Geoscience*

the destructive powers of rock avalanches are unprecedented. They are exceptional hazards produced when very large rockslides disintegrate during transport (Hungr et al., 2013), and are often recognized as very fast moving, dry granular flows (Lucas et al., 2014). The travel distance of the deposit front, or runout, is an important measure for their hazard assessment (Vaunat and Leroueil, 2002), and is generally found to be very large compared to their fall height (Hsü, 1975). This suggests very low effective basal friction, which is usually attributed to a reduced normal stress at the base, and various mechanisms have been proposed which can lead to this (e.g. Kent, 1966; Shreve, 1968; Hsü, 1975; Melosh, 1979; Campbell, 1989). For convenience, the reduction in basal friction can be considered through an effective coefficient of friction, μ_{eff}, which emerges naturally when considering energy conservation of the simple case of a rigid block of mass M sliding down a planar slope

$$MgH' = \mu_{eff} MgL' \Rightarrow \mu_{eff} = \frac{H'}{L'} \tag{5.1}$$

where H' and L' is the vertical and horizontal displacement of the block, respectively. Unlike a block, however, a rock avalanche may deform and spread. Additionally, field observations of the displacement of rock avalanches are often given by vertical (H) and horizontal (L) distance from the deposit's front with respect to the top of the main scarp (Figure 5.1). The resulting ratio

$$\mu_{ap} = \frac{H}{L} \tag{5.2}$$

is known as the Heim's ratio (Heim, 1882, as cited in Hsü, 1975), or the apparent coefficient of friction (Manzella and Labiouse, 2012), and serves as a proxy for μ_{eff}.

Though very noisy, one of the best established, but perhaps least understood observation of rock avalanches is the dependence of the Heim's ratio on volume: rockslides below a size of approximately 10^6 m^3 all have a relatively constant Heim's ratio of ∼0.4-0.7, but for larger rockslides it decreases with volume, reaching values <0.1 for volumes larger than 10^9 m^3 (Lucas et al., 2014). This suggests a scale-dependent mechanism, causing decreasing apparent friction with volume, which is only relevant for the large volume rockslides (Davies and McSaveney, 1999). Whether also the effective friction depends on volume is uncertain, though the recent analysis by Lucas et al. (2014) suggests this too is dependent on volume.

The uncertainty lies in the fact that the runout is defined by the front of the deposits, and therefore contains the combined effect of both translation and spreading of the rock mass. The additional travel distance from spreading can have profound effect on the runout (Staron and Lajeunesse, 2009), especially if the effective basal friction is low. Though often not explicitly considered, the process of fragmentation can play a crucial role in the spreading of rock avalanches (Bowman et al., 2012). Firstly, one may expect that the finer the material, the more flow-like the behavior, allowing the rock mass to spread more easily (Locat et al., 2006). Secondly, experimental models of fragmenting rockslides suggest that dynamic fragmentation actively increases the spreading (Bowman et al., 2012; Haug et al., under review JGR). Field observations have also indicated an important role played by fragmentation: Hungr et al. (2013) pointed out that the mobility of some rock avalanches, e.g. the Great Fall of Folkestone

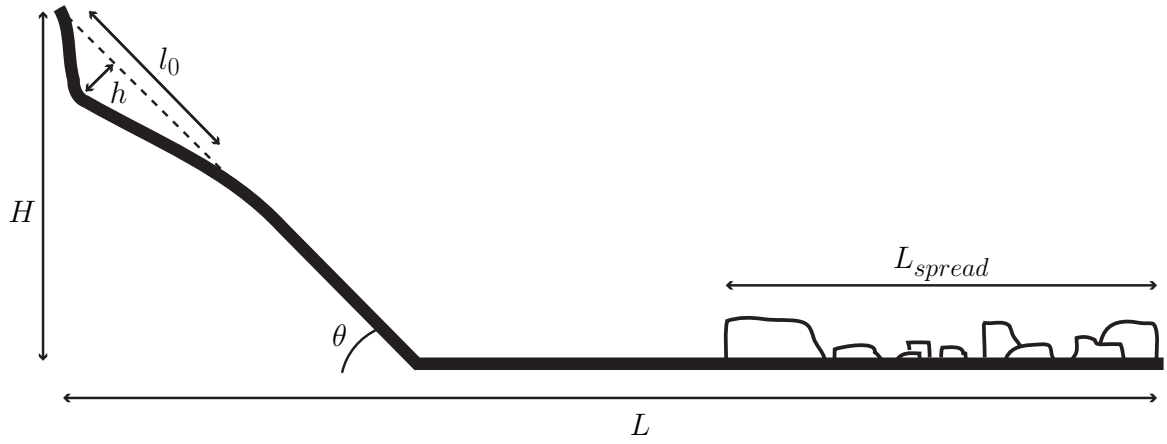

Figure 5.1: **Sketch of the slope geometry of experiments and various length measurements**

Warren (Hutchinson et al., 1980), may possibly be promoted by the dynamic fragmentation of brittle cap rock. In fact, the lack of any dynamic fragmentation events may very well inhibit a high mobility: the Randa rockslide in Switzerland was observed to immediately disintegrate and collapse during slope failure, which was interpreted by Eberhardt et al. (2004) to cause its relatively short runout, despite being of considerable size. In spite of these indications, investigations of nine rock avalanches by Locat et al. (2006) revealed no correlation between the degree of fragmentation and the runout.

Field observations of the degree of fragmentation and its effect on rock avalanches are sparse. Modeling therefore serves as a valuable tool for studying these systems. Typically, fragmentation is not considered in rock avalanche models, which commonly either assume a block model with an effective basal coefficient of friction (e.g. Yang et al., 2014), or a granular model (e.g. Manzella and Labiouse, 2012). Mostly, the underlying assumption is that all fragmentation occurred at the time of the slope failure (static fragmentation), and that this fragmentation event has negligible effect on the energy budget and the kinetics of the slide. Natural rock avalanches do not, however, always fit into such simplifying assumption. A typical rock avalanche can initially start out as a more or less intact rock, before undergoing dynamic fragmentation during slope failure and transport (Locat et al., 2006).

We performed analogue models of dynamically fragmenting rock avalanches (Figure 5.1). We hypothesize that there exists some mechanism, whatever it may be, that causes a low, but constant effective coefficient of friction. This entails that any variation in Heim's ratio is the result in variations of the degree of fragmentation. We expect the effective friction coefficient to always be larger than the apparent one, i.e. $\mu_{eff} > \mu_{ap}$. Since the apparent friction coefficient goes down to approximately 0.1 (Lucas et al., 2014), we implemented in our models a basal friction coefficient of 0.15 (Haug et al., under review JGR).

Figure 5.2 presents snapshots from two experiments of different degree of fragmentation.

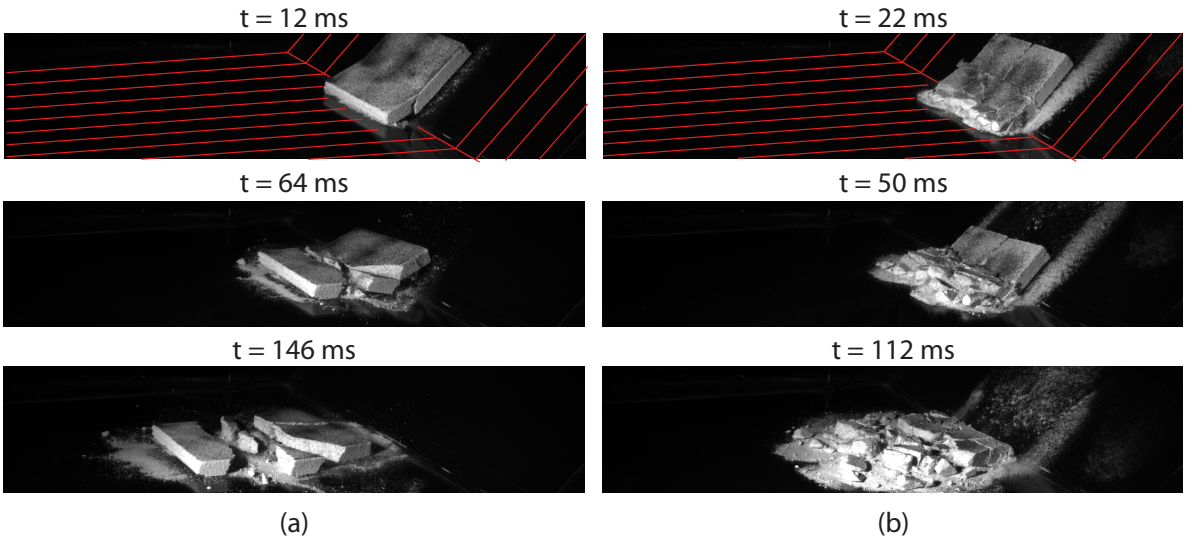

Figure 5.2: **Snapshots from the experiments**: (a) intermediate strength sample ($C = 40\,\text{kPa}$) and (b) low strength sample ($C = 4\,\text{kPa}$). The stronger sample (a) breaks apart into six large fragments, with limited amount of fine-grained material produced, which after breaking move apart with little interaction. In contrast, the weaker sample fragments into many small pieces, with a large fraction of fine-grained material, which interact more strongly. The red lines in the upper images indicate the geometry of the basal plates. The time given above each image reflects the time since first impact.

Observations of these models reveal that not only the size and number of fragments are different, but that a higher degree of internal deformation and friction is experienced with increased fragmentation.

The Heim's ratio for experiments with different degrees of fragmentation (m_c) is plotted in Figure 5.3a. It shows that the runout increases for low to intermediate degrees of fragmentation, reaching a maximum (lowest Heim's ratio) for $m_c \approx 5$. With further increase of fragmentation an increase in Heim's ratio, i.e. decreased runout, is observed. A similar behavior is observed for the length of the deposits (Figure 5.3b), which increase until $m_c \approx 5$, before it decreases for higher values. Importantly, the lowest apparent basal friction, equivalent to the lowest Heim's ratio, is close to the implemented effective basal friction. Therefore, all processes operating in our models (e.g. fragmentation, internal friction between fragments) tends to consume energy and thereby reduce runout from its optimum.

The increasing runout with m_c for the low degrees of fragmentation ($m_c < 5$) observed in Figure 5.3a, is caused by an increased spreading with fragmentation (Figure 5.3b). A similar result was also obtained by previous analogue models (Bowman et al., 2012; Haug et al., under review JGR). In contrast to these studies, we show here that the runout is not simply increasing with the degree of fragmentation, but that it displays an optimum for $m_c \approx 5$. Considering

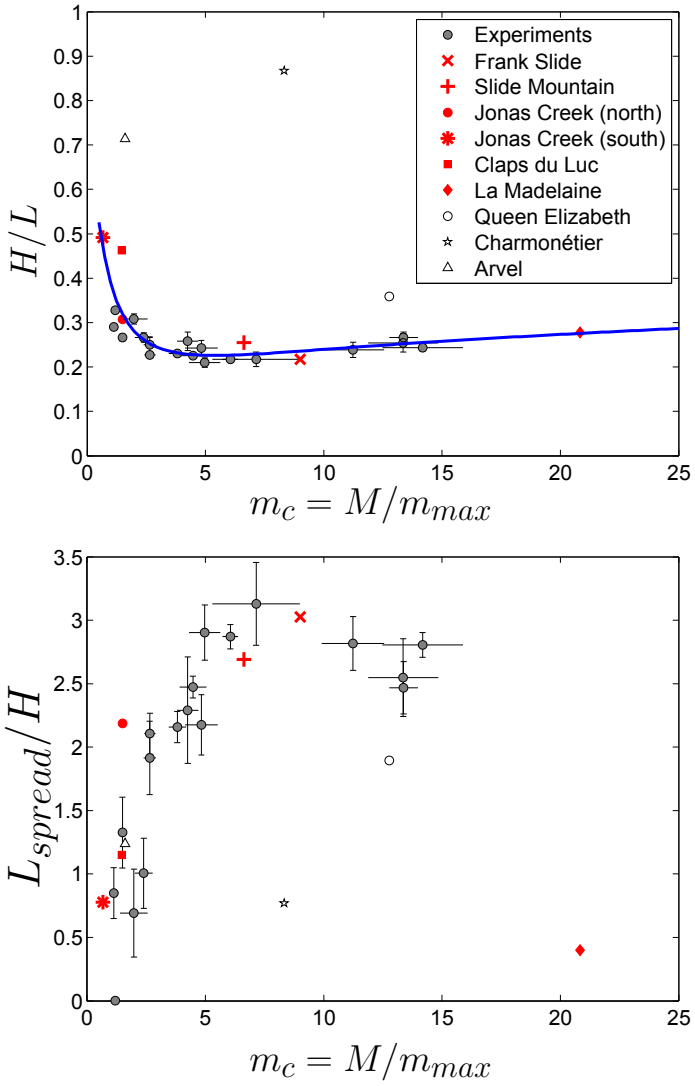

Figure 5.3: **Heim's ratio and deposit length of models compared to natural rock avalanches presented Locat et al. (2006)**. (a) The Heim's ratio of the analogue models (gray) and from the rock avalanches (red = selected set, open = discarded). The blue line represents the best fit of Equation 5.3, with parameters $\alpha = 0.12$, $\beta = 0.97$ and $\gamma = 1.7$. (b) The deposits length. The gray circles represent the average value of a set of 4-15 experiments and the error bars give the standard error of the set.

the increased internal friction with the degree of fragmentation (Figures 5.2), the reduction of runout with $m_c > 5$ appears to be the result of the increased energy dissipation through internal friction. Consequently, the minimum of the Heim's ratio observed in Figure 5.3a is the result of a competition between spreading and internal friction.

We compare our experimental results (Figure 5.3) with data from nine rock avalanches reported by Locat et al. (2006), which show no clear volume dependence of runout. This makes this data set ideal to test whether a scale-independent process is operating besides dynamic basal weakening. Further, not all the rock avalanches reported in (Locat et al., 2006) are comparable to our experimental setup by means of material properties and geometries (Figure 5.1). Based on the slope geometry, the Queen Elizabeth slide is discarded because of its run-up on the opposite valley wall. Also discarded is the Charmontétier slide, because of the sudden free fall stage at the end of its transport. Additionally, the Arvel slide was observed to bulldoze soft material in front of it, such complexities are not considered in our models and this one is also neglected.

Figure 5.3 display a remarkable fit between the experimental and the selected natural data. The data points from Jonas Creek (north) and Clapse du Luc are observed to extend the trend from the experiments to higher Heim's ratio for low degrees of fragmentations: The good fit of these slides with the deposit lengths (Figure 5.3b) suggests this extension of the trend in Heim's ratio is true. La Madelaine slide is observed to nicely follow the trend of the experimental results of Heim's ratio to higher degrees of fragmentation. If this point is indeed the continuation of the trend, its very low spreading value (Figure 5.3b) suggests that the reduction of spreading indicated by the experiments for $m_c > 5$ continues for even higher degrees of fragmentation. Based on the conservation of energy, the runout can be described mathematically (see supplementary material) by

$$\frac{H}{L} = \mu \left(1 + \frac{\mu}{\sin\theta}\left(1 - \cos\theta\right) - \alpha log(m_c) - \beta e^{-m_c/\gamma}\right)^{-1} \tag{5.3}$$

where α, β, and γ are constants, which illustrates the competition between spreading ($\beta e^{-m_c/\gamma}$) and the increasing energy dissipation ($\alpha log(m_c)$) with m_c. The Heim's ratios of the neglected slides are all, as expected, higher than the selected data set for their respective degrees of fragmentation, illustrating the importance also of topography (e.g. opposite valley wall), and complexities such as bulldozing.

The good fit between experimental and natural data suggests that the rock avalanches considered here have a close to constant effective friction at about 0.15. This implies that over a range of two orders of magnitude (from $2 \cdot 10^6$ to $90 \cdot 10^6$ m^3), the effective coefficient of friction of rock avalanches is independent of volume. Consequently, our results show that fragmentation plays a governing role in the runout of rock avalanches. Interestingly, the good fit shown here suggests that the runout is independent of the mechanism of fragmentation, which is elastic bending in the models (Haug et al., under review JGR) and likely grinding and comminution for rock avalanches (Crosta et al., 2007), and simply determined by the degree of fragmentation.

Our results show that under similar conditions, a fragmenting "strong" rock will travel further than a deforming "weak" rock. Fragmentation of a strong rock increases runout through spreading, which may explain why the brittle fragmentation of strong cap rock is related to some long runout rock avalanches, e.g. the Great Fall of Folkestone Warren (Hungr et al., 2013; Hutchinson et al., 1980). On the other hand, collapse of a weak rock dissipates energy very efficiently due to the intensive internal deformation. This may be coincident with the relatively short travel distance of the Randa rockslide (Eberhardt et al., 2004). We conclude that the runout of rock avalanches might be dominated by variation in fragmentation, not basal weakening. Because fragmentation is controlled by rock strength, the substantial noise in the volume dependence of runout related to dynamic basal weakening may be caused by that rock strength, not volume, is the primary controlling parameter. Consequently, because of the dominating role of fragmentation in the runout of rock avalanches, it should be included in their hazard assessments.

Methods

In the experiments, a cuboid sample of a rock analogue material is accelerated down a glass plate held at an angle of 45° with the horizontal (Figures 5.1). After 1 meter of travel, the sample impacts on a horizontal plate, causing it to fragment. Once the sample has moved onto the horizontal plate, the fragmented material spreads and finally comes to rest. The analogue material is cemented fluvial quartz sand. It is produced by mixing water and gypsum or potato starch into the sand, which is left to set for 2 days (in case of gypsum cement) or heated for 15 minutes in a 900 W microwave (in case of potato starch cement). The cohesion of the material can be controlled by the type and the amount of cement added to the mixture, allowing control of the strength of the material over several orders of magnitude (Haug et al., 2014).

The main observables from the experiments are the mass of the largest fragment (m_{max}), and travel distance of the front (L) of the final deposits. The front is determined by the mass-weighted average position of the most distal 5 % of total mass. This defines a frontal rim which is a more robust runout estimate than using simply the foremost fragment position.

Typically, the fragmentation is characterized through the fragment size distribution (e.g. Crosta et al., 2007); however, it is difficult to evaluate the distribution if too few fragments are produced, i.e. for low degrees of fragmentation. To overcome this, we determine the degree of fragmentation from the characteristic fragment size $m_c = M/m_{max}$ (Timár et al., 2012), where m_{max} is the mass of the largest fragment and M is the mass of the sample. A value of $m_c \approx 1$ characterizes a sample which might be slightly damaged, but intact, while an increasing value represents an increasing degree of fragmentation. In comparison, Locat et al. (2006) consider the relative change of the 50 % quartiles of the size distribution before and after the transport event, as a measure of the degree of fragmentation. In similar terms, since our parameter m_c considers the mass of the initial sample and the largest fragment, it is equivalent to the relative change of the 100 % quartile. However, because the shapes of distributions reported

by Locat et al. (2006) are the same before and after the movement, the ratio of any quartile for the two respective distributions is constant, such that a direct comparison between their measure and our m_c is justified.

Here we report on the results from two series of experiments. (1) In one series of experiments we test the effect of the thickness to length ratio ($h/l_0 = 0.033 - 0.49$) of the samples while keeping the cohesion constant at $C = 14$ kPa. (2) In another series of experiments we vary the cohesion of the material $C = 4 - 350$ kPa while keeping the thickness to length ratio constant at $h/l_0 = 0.13$. In all experiments, the release height is kept constant at 0.71 m. The results of these experiments reveal that the runout of fragmenting rockslides depends on the degree of fragmentation in a complex manner. To gain more insight into the process of fragmentation, the fragmentation of two samples with different cohesions ($C = 4$ and 40 kPa, $h/l_0 = 0.13$) is considered using a camera with a frame rate of 500 Hz. These two experiments have a fall height of 0.35 m.

References

K. J. Hsü. Catastrophic debris streams (sturzstroms) generated by rockfalls. *Geological Society of America Bulletin*, 86(50117):129–140, 1975. URL `http://bulletin.geoscienceworld.org/content/86/1/129.short`.

O. Hungr, S. Leroueil, and L. Picarelli. The Varnes classification of landslide types, an update. *Landslides*, 11(2):167–194, November 2013. doi: 10.1007/s10346-013-0436-y.

P. E. Kent. The transport mechanism in catastrophic rock falls. *The Journal of Geology*, 74(1):79–83, 1966. URL `http://www.jstor.org/stable/10.2307/30075179`.

R. L. Shreve. Leakage and fluidization in air-layer lubricated avalanches. *Geological Society of America Bulletin*, 79(5):653–658, 1968. doi: 10.1130/0016-7606(1968)79. URL `http://bulletin.geoscienceworld.org/content/79/5/653.short`.

H. J. Melosh. Acoustic Fluidization : A New Geologic Process? *Journal of Geophysical Research*, 84(9):7513–7520, 1979.

C. S. Campbell. Self-lubrication for long runout landslides. *The Journal of Geology*, 97 (6):653–665, 1989. URL `http://www.jstor.org/stable/10.2307/30062196`.

L. Staron and E. Lajeunesse. Understanding how volume affects the mobility of dry debris flows. *Geophysical Research Letters*, 36(12):2–5, June 2009. ISSN 0094-8276. doi: 10.1029/2009GL038229. URL `http://www.agu.org/pubs/crossref/2009/2009GL038229.shtml`.

A. Lucas, A. Mangeney, and J. P. Ampuero. Frictional velocity-weakening in landslides on Earth and on other planetary bodies. *Nature communications*, 5:3417, January 2014. ISSN 2041-1723. doi: 10.1038/ncomms4417. URL `http://www.ncbi.nlm.nih.gov/pubmed/24595169`.

J. Vaunat and S. Leroueil. Analysis of Post-Failure Slope Movements within the Framework of Hazard and Risk Analysis. *Natural Hazards*, pages 83–109, 2002. ISSN 0921030X.

A. Heim. Der bergsturz von elm. *Zeitschrift der Deutschen Geologischen Gesellschaft*, pages 74–115, 1882.

I. Manzella and V. Labiouse. Empirical and analytical analyses of laboratory granular flows to investigate rock avalanche propagation. *Landslides*, (January), January 2012. ISSN 1612-510X. doi: 10.1007/s10346-011-0313-5.

T. R. Davies and M. J. McSaveney. Runout of dry granular avalanches. *Canadian Geotechnical Journal*, 36(2):313–320, 1999. doi: 10.1139/t98-108.

E. T. Bowman, W. A. Take, K. L. Rait, and C. Hann. Physical models of rock avalanche spreading behaviour with dynamic fragmentation. *Canadian Geotechnical Journal*, 49(4): 460–476, 2012. doi: 10.1139/t2012-007.

P. Locat, R. Couture, S. Leroueil, J. Locat, and M. Jaboyedoff. Fragmentation energy in rock avalanches. *Canadian Geotechnical Journal*, 43(8):830–851, 2006. doi: 10.1139/t06-045.

Ø. T. Haug, M. Rosenau, K. Leever, and O. Oncken. Effect of fragmentation on the runout of gravitational mass movements: insights from analogue experiments. *Journal of Geophysical Research*, under review JGR.

J. N. Hutchinson, E. N. Bromhead, and J. F. Lupini. Additional observations on the Folkestone Warren landslides. *Quarterly Journal of Engineering Geology and Hydrogeology*, 13:1–31, 1980.

E. Eberhardt, D. Stead, and J. S. Coggan. Numerical analysis of initiation and progressive failure in natural rock slopes – the 1991 Randa rockslide. *International Journal of Rock Mechanics and Mining Sciences*, 41(1):69–87, January 2004. ISSN 13651609. doi: 10.1016/S1365-1609(03)00076-5. URL `http://linkinghub.elsevier.com/retrieve/pii/S1365160903000765`.

C.-M. Yang, W.-L. Yu, J.-J. Dong, C.-Y. Kuo, T. Shimamoto, C.-T. Lee, T. Togo, and Y. Miyamoto. Initiation, movement, and run-out of the giant Tsaoling landslide – What can we learn from a simple rigid block model and a velocity-displacement dependent friction law? *Engineering Geology*, 182:158–181, November 2014. ISSN 00137952. doi: 10.1016/j.enggeo.2014.08.008. URL `http://linkinghub.elsevier.com/retrieve/pii/S0013795214002075`.

G. B. Crosta, P. Frattini, and N. Fusi. Fragmentation in the Val Pola rock avalanche, Italian Alps. *Journal of Geophysical Research*, 112:F01006, February 2007. doi: 10.1029/2005JF000455.

Ø. T. Haug, M. Rosenau, K. Leever, and O. Oncken. Modelling Fragmentation in Rock Avalanches. *Landslide Science for a Safer Geo-Environment*, 2, 2014. doi: 10.1007/978-3-319-05050-8_16.

G. Timár, F. Kun, H. a. Carmona, and H. J. Herrmann. Scaling laws for impact fragmentation of spherical solids. *Physical Review E*, 86(1):016113, July 2012. ISSN 1539-3755. doi: 10.1103/PhysRevE.86.016113. URL `http://link.aps.org/doi/10.1103/PhysRevE.86.016113`.

Supplementary material: A mathematical description of the dependence on fragmentation of Heim's ratio

Generally, the conservation of energy of a sliding mass M requires that

$$MgH = \mu MgL_p + W \tag{5.4}$$

where g is the gravitational acceleration, H is the vertical fall height, and L_p is the entire travel path of the slide and W is the sum of any other energy dissipating terms. Here, we have assumed Coulomb friction at the base. For the geometry of our experimental setup up (i.e. Figure 5.1), and also roughly for the set of selected rock avalanches, the L_p can be expressed in terms of the horizontal runout L as

$$L_p = L + L_s(1 - \cos\theta) - \frac{1}{2}l_0\cos\theta - \frac{1}{2}L_{spread} \tag{5.5}$$

where L_s is the length and θ the angle of the slope, l_0 is the initial length of the slide, and where it is assumed that the additional travel length due to spreading is equal to half the deposit length. Since the term including the initial length is expected to be very small compared to the other terms, it is neglected in the further analysis. Inserting this expression into Equation 5.4 and solving for L gives

$$L = \frac{H}{\mu} - L_s(1 - \cos\theta) + \frac{1}{2}L_{spread}(\mu, \phi, m_c, W) - W(\mu, \phi, m_c) \tag{5.6}$$

where it is emphasized that both L_{spread} and W is expected to be functions of the basal friction, μ, internal friction, ϕ, the degree of fragmentation, m_c, as well as a possible non-linear dependence between L_{spread} and W. With this expression for the runout, the Heim's ratio is

$$\frac{H}{L} = \mu\left(1 + \frac{\mu}{\sin\theta}(1 - \cos\theta) + \frac{L_{spread}(\mu, \phi, m_c, W)}{2H} - \frac{W(\mu, \phi, m_c, L_{spread})}{MgH}\right)^{-1} \tag{5.7}$$

A direct determination of the two last terms in Equation 5.7 is difficult, however, from the experimental work by Haug et al. (under review JGR), we know that W/Mgh can be described with a logarithmic function of m_c. Additionally, based on the shape of both the Heim' ratio and the L_{spread} plotted in Figure 5.3, it appears that it can be reasonably be described by an exponential function of m_c. This leads to the approximation that

$$\frac{L_{spread}(\mu, \phi, m_c)}{2H} - \frac{W(\mu, \phi, m_c)}{MgH} = -\alpha log(m_c) - \beta e^{-m_c/\gamma} \tag{5.8}$$

such that the Heim's ratio can be expressed as

$$\frac{H}{L} = \mu \left(1 + \frac{\mu}{\sin\theta}\left(1 - \cos\theta\right) - \alpha log(m_c) - \beta e^{-m_c/\gamma}\right)^{-1} \tag{5.9}$$

Chapter 6

Conclusions

I have designed a new analogue material that allows for realistic modeling of fragmentation in gravitational rock movements at a laboratory-scale. Samples of this material are released down a chute and monitored using digital cameras. I have developed an image analysis tool in Matlab that can extract the relevant data from the experiments, allowing for a quantitative analysis of the fragmentation of rockslides.

The experimental results reveal that the process of fragmentation consumes energy at the cost of the travel distance of the center of mass. Nevertheless, the fragmentation also causes an increased amount of spreading of the deposits, leading to an increased runout for fragmenting systems. However, the runout is observed to depend on the degree of fragmentation in a complex manner, increasing with moderate degrees of fragmentation, but decreasing if above an optimum. The complex dependence on the degree of fragmentation reflects the competition between spreading and internal friction.

The degree of fragmentation depends on the kinetic energy before impact, the cohesion of the material and the geometry of the sample. To understand the relative importance of each variable and how they are related, an analytical model is considered that leads to a parameter which includes all of these variables. This allows for the establishment of one simple scaling law, relating the initial conditions to the final degree of fragmentation. Such a scaling law can prove very helpful in predicting both the degree of fragmentation and the dominating mode of transport of rockslides.

Comparing the experimental models presented here to a set of nine natural rock avalanches reveals that for similar topographies the runout follows the same trend with the degree of fragmentation. This shows that fragmentation is a governing mechanism for the runout of rock avalanches. Consequently, variation of the degree of fragmentation, as well as of topography, may be at the origin of the large scatter in the classical runout-volume plots.

Chapter 7

Outlook

Though this work has established some of the effects of fragmentation on the transport of rockslides, there are certainly many stones left unturned, some of which I present here.

One of the biggest limitation of the experimental models presented in this thesis is the neglect of pre-existing fractures within the sample. Even though the change of bulk cohesion can remedy this somewhat by modeling the effectively lower strength of a heavily fractured material, there are kinetic differences which cannot be considered with such an approach. Was I to make one more series of experiments, I would prepare samples consisting of several small blocks, and systematically vary the size of the blocks with respect to the total size of the slide.

An interesting possible outcome of such a study, apart from the direct study of the system, is to compare the pre-fractured sample with the variation of bulk cohesion. Perhaps, by comparing variables such as the travel distance (i.e. the center of mass) or the runout (i.e. the front of the deposits), one can make a comparison with the equivalent bulk cohesion tests, yielding a pre-fractured sample's effective bulk cohesion. That is, if a given pre-fractured sample has similar travel distance and runout as a given bulk cohesion sample, one could make the argument that they are kinetically similar, and therefore equivalent. Such an analysis could also be interesting for the generally difficult task of determining effective properties of fractured rock.

Rather than preparing experimental slides consisting of small blocks, however, perhaps a more realistic approach would be to re-fragment a fragmented sample by releasing a sample several times. Though, with more realism comes more complications, and for such an approach one would need good control of the fragment size distribution.

Another interesting issue is related to the time of the fragmentation event. In the current setup, the fragmentation always occurs at the same time, followed by horizontal sliding and spreading. However, if the fragmentation event would occur earlier, i.e. somewhere along the slope, one could expect the outcome to be different. An example that illustrates this can be seen from the comparison between the sand experiments and the cohesive ones in Chapter 2: since the "fragmentation event" of the sand experiments occurs immediately at release, they behave kinematically different to the cohesive sample. If a fragmentation event of a cohesive

sample is followed by another acceleration stage, one may perhaps expect a similar behavior to the sand experiments.

Finally, perhaps the most difficult task in the study of the effect of fragmentation in gravitational rock movements is related to the lack of data from nature. Here, I have compared the models presented in this thesis with a total of nine rock avalanches. Additional data, not only from rock avalanches but also from smaller rockslides, would prove beneficial for further analysis. Therefore, perhaps the most important extension of the current work would be a data base containing a measure of the degree of fragmentation, travel distances and runouts of more rock avalanches and rockslides.

Chapter 8

Acknowledgments

Many thanks to my supervisors: Matthias Rosenau, Karen Leever and Onno Oncken, whose help and guidance during these three years has been crucial for the completion of this project. Also many thanks to my own personal government: Elvira, for keeping me in line both technically, grammatically and personally. The work presented here would not be possible without the skills of Frank Neumann and Thomas Ziegenhagen, that helped build and design the experimental setups. Finally, a big "thank you" goes out to the PhD students in section 3.1 (+ Iskander), for that rather not so professional part of my German years, but for making it all the more interesting.

This work was supported by the Helmholtz Graduate Research School GEOSIM and the German Ministry for Education and Research (BMBF, FKZ03G0809A).

For reasons of data protection, the Curriculum Vitae is not published in the electronic version.

For reasons of data protection, the Curriculum Vitae is not published in the electronic version.

For reasons of data protection, the Curriculum Vitae is not published in the electronic version.